Southampton
Oceanography
Centre

Report

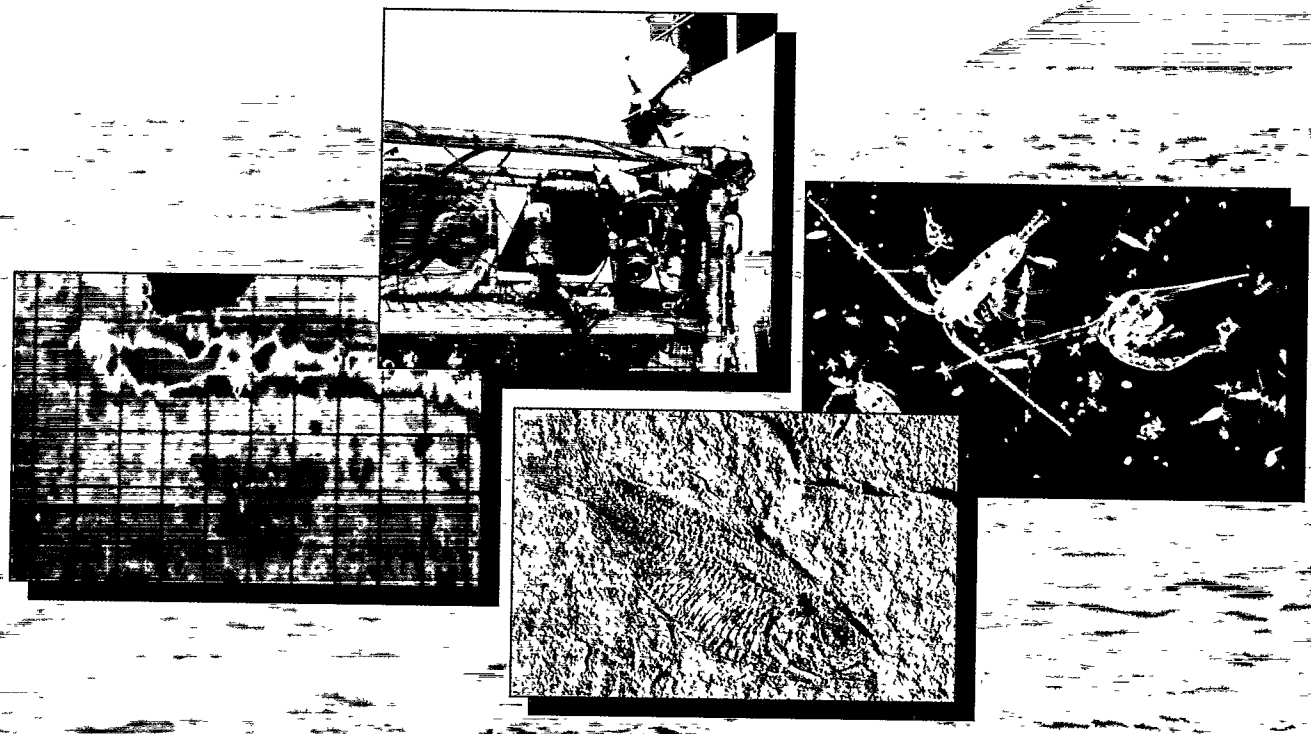

Natural
Environment
Research
Council

University
of Southampton

SOUTHAMPTON OCEANOGRAPHY CENTRE

REPORT No. 6

The Southampton Oceanography Centre (SOC) Ocean - Atmosphere Heat, Momentum and Freshwater Flux Atlas

S A Josey, E C Kent & P K Taylor

1998

James Rennell Division for Ocean Circulation and Climate
Southampton Oceanography Centre
University of Southampton
Waterfront Campus
European Way
Southampton
Hants SO14 3ZH UK
Tel: +44 (0)1703 596409
Fax: +44 (0)1703 596400
Email: S.A.Josey@soc.soton.ac.uk

DOCUMENT DATA SHEET

AUTHOR

JOSEY, S A, KENT, E C & TAYLOR, P K

PUBLICATION DATE

1998

TITLE

The Southampton Oceanography Centre (SOC) Ocean - Atmosphere Heat, Momentum and Freshwater Flux Atlas.

REFERENCE

Southampton Oceanography Centre Report, No. 6, 30pp. & figs.

ABSTRACT

Global climatological fields of the monthly mean air-sea fluxes of heat, momentum and freshwater are presented in this atlas. The fields have been calculated at the Southampton Oceanography Centre from a data set of marine meteorological reports spanning the period 1980 - 1993 which has been corrected for biases arising from variations in observing procedure. The dataset is a modified version of the Comprehensive Ocean - Atmosphere Dataset 1a onto which we have merged data describing observation method from the International List of Selected, Supplementary and Auxiliary Ships (the WMO Report 47). The primary purpose of this document is to detail the method by which the fluxes were calculated and present an overview of the climatological monthly mean fields. In addition, the impact of the observing procedure corrections on the monthly mean flux fields has been quantified and is shown to be up to 15 Wm^{-2} with strong seasonal and regional variations.

The climatological fields are freely available to interested users for non-commercial scientific research, for details of how to access the fields see:
http://www.soc.soton.ac.uk/JRD/MET/fluxclimatology.html.

KEYWORDS

CLIMATOLOGY, COAD, DATA COLLECTION, FRESHWATER FLUX, HEAT EXCHANGE, METEOROLOGICAL DATA, MOMENTUM EXCHANGE, SELECTED SHIPS, WATER EXCHANGE, WIND STRESS

ISSUING ORGANISATION

Southampton Oceanography Centre
University of Southampton
Waterfront Campus
European Way
Southampton SO14 3ZH
UK

Director: Professor John Shepherd

Copies of this report are available from: **National Oceanographic Library, SOC** *PRICE*: £16.00

Tel: +44(0) 01703 596116 Fax: +44(0) 01703 596115 Email: nol@soc.soton.ac.uk

TABLE OF CONTENTS

1. Introduction

Air-sea fluxes of heat, momentum and freshwater are key components of the coupled ocean-atmosphere system. Climatological analyses of these exchange fields have relied to a large extent on meteorological reports from merchant ships at sea with a number of flux atlases being produced from such data (e.g. Bunker, 1976 ; Esbensen and Kushnir, 1981; Oberhuber, 1988 ; da Silva et al., 1994). However, the ship reports used in these analyses are known to contain biases arising from variations in observing procedure (Kent et al., 1993). Previous to this study, the task of systematically correcting for these biases at the level of the individual reports needed to calculate the fluxes had not been undertaken. In this atlas, we present for the first time global climatological fields of the air-sea fluxes of heat, momentum and freshwater which have been derived from corrected meteorological reports. The fields have been generated at the Southampton Oceanography Centre (SOC) from a dataset of marine meteorological reports spanning the period 1980 - 1993. The climatology is freely available to interested users for non-commercial scientific research, for details of how to access the fields see http://www.soc.soton.ac.uk/JRD/MET/fluxclimatology.html.

In order to allow corrections to be made for observational bias we have combined information describing observation method from the annually published WMO47 list of ships (e.g. WMO, 1993) with our primary dataset of in situ reports, the Comprehensive Ocean - Atmosphere Dataset 1a (COADS1a, Woodruff et al., 1993). There is sufficient information in the resulting combined dataset to allow various corrections for observational bias to be made. The corrections employed were developed in an earlier intensive study of merchant ship characteristics in the North Atlantic (Kent and Taylor, 1991; Kent et al., 1991 ; Kent et al., 1993ab). The results of a number of supporting studies have been used to determine several key components of the flux calculation process including the visual wind estimate conversion scale (Kent and Taylor, 1997), the longwave flux formula (Josey et al., 1997) and the method employed to average the flux fields (Josey et al., 1995).

The accuracy of the individual monthly flux fields has been assessed using high quality research buoy measurements at several climatically different locations. On a larger scale, box mean surface heat fluxes derived from hydrographic section data have been compared with the corresponding SOC values giving further insight into regional biases within the climatology. The results of these evaluation studies are published in Josey et al. (1999) and we do not discuss them in detail within this atlas, the primary purpose of which is to document the method by which the fluxes were calculated and present an overview of the climatological monthly mean fields.

The global distribution of ship reports is spatially inhomogeneous with a relatively large number of observations in the mid-latitude North Atlantic and North Pacific but very few in the Southern Hemisphere. Despite the limitations imposed by this distribution we believe that climatological analysis of fluxes derived from ship observations can provide useful information. Satellite and NWP model derived fluxes potentially offer full global coverage but suffer from other disadvantages. Satellite estimates of the latent heat and shortwave fluxes are improving in quality (Schulz et al., 1997 ; WCRP/GEWEX, 1996) but retrieval of the longwave flux remains problematic and as yet no useful technique has been advanced for retrieving surface air temperature, hence the sensible heat flux cannot reliably be estimated. Estimates of the surface fluxes from NWP models suffer from continuing uncertainties over model physics, particularly with regard to the representation of clouds, and significant differences remain between the output from the various reanalysis programs.

The datasets from which the climatology has been generated are described in the following section. In Section 3, the method by which the individual heat flux estimates have been obtained and the analysis procedure used to produce the climatological mean fields are detailed. In Section 4, we give an overview of the main characteristics of the heat flux fields and the impact of the corrections for observational bias. Finally, we discuss outstanding problems and possible future improvements to the climatology.

2. Source Datasets

The dataset that forms the basis of the climatology is the global Comprehensive Ocean-Atmosphere Dataset (COADS) Release 1a (Woodruff et al., 1993) with extensions, which in total covers the period 1980 - 1993. The full dataset contains some 30 million in situ meteorological reports. Its composition changes significantly throughout the period considered with reports from the Coastal Marine Automated Network (C-MAN), drifting and moored buoys dominating towards the end. The reliability of the C-MAN and drifting buoy reports has been questioned and prior to our analysis we have removed reports in these classes together with moored buoy reports that occur at intervals shorter than three hours.

In order to apply the bias corrections described in the following section, additional metadata regarding the observing procedures used on specific ships has been merged onto the COADS1a from the International List of Selected, Supplementary and Auxiliary Ships (the WMO Report 47, e.g. WMO, 1993) which is published annually by the World Meteorological Organisation (WMO). The report contains details of the instrumentation carried on most of the approximately 7000 Voluntary Observing Ships. In our analysis we have made use of metadata

describing the height at which the anemometer was deployed and the height of the observing platform (the latter being used as a proxy for the temperature and humidity sensor heights) and the method by which the sea surface temperature and the atmospheric humidity were measured.

The COADS1a and WMO47 list were merged using the ship callsign which is common to each dataset. For each report within the COADS1a, the WMO47 file for the corresponding year was searched for the listed callsign. If the callsign was present in the WMO47 file, the metadata for that particular ship was appended to the COADS1a report. If not the procedure was repeated for the WMO47 files for the following two years and finally for the preceding year. If no matching callsign was found absent data were appended to the report. We are aware that call signs may occasionally be transferred between ships but are unable to correct for this at present.

Time series of the total number of reports, the number made by ships and the number that have been matched in the merged dataset are shown in Fig.1. The proportion of reports for which matching was successful increased throughout the time period considered, typical values being 43% in January 1980 and 70% in January 1990. The reason for the trend is that the proportion of valid callsigns in COADS rises throughout the period although it is countered to some extent by the increasing proportion of buoy reports in the dataset. No attempt has been made to include additional metadata for the buoys as there is currently no comprehensive dataset describing their characteristics.

3. Flux Calculation Method

3.1. Corrections to the Reported Fields for Systematic Errors

The existence of systematic biases in surface meteorological observations made by Voluntary Observing Ships (VOS) which form the core of the reports contained in COADS1a has been identified within the VOS Special Observing Project for the North Atlantic (VSOP-NA, Kent and Taylor, 1991 ; Kent et al., 1991 ; Kent et al., 1993ab). In that study, detailed information regarding observing procedure was collected for a subset of the VOS fleet reporting in the North Atlantic and corrections developed for various observational biases by using NWP model analysis output as a means of intercomparison. We have applied these corrections to the reported meteorological observations, before calculating the heat fluxes, as follows:

i.) Sea surface temperature (SST) measurements made with a thermometer situated in the engine cooling system are reduced by 0.35^{o} C. If no information was available about the method of SST measurement a default correction of 0.2^{o} C was applied since the WMO47 list indicated that the proportion of ships making engine inlet measurements was about 60 %.

ii.) Humidity measurements made using un-aspirated screens have been corrected as follows,

$$T_{Dew}^{C} = 1.029 T_{Dew} - 1.080 \quad (1)$$

where T_{Dew}^{C} and T_{Dew} are the corrected and uncorrected dew point temperatures respectively with units ^{o}C. A default correction equal to one third of that given by (1) was applied if no information was available about the method of humidity measurement, based on the proportion of ships making un-aspirated screen measurements which was about 30 %.

iii.) Air temperatures have been reduced by an amount ΔT_{rad} in ^{o}C for heating of the ship environment by solar radiation (Kent et al., 1993b) where ,

$$\Delta T_{rad} = (2.7 - 0.064\ u_{rel})\ Q_{SW} / 1000 \quad (2)$$

in which Q_{SW} (units Wm^{-2}) is the incoming shortwave calculated using the Dobson and Smith (1988) 'okta' model detailed in 3.2.4 and u_{rel} (units ms^{-1}) the wind speed relative to the ship, which has been determined using the ship speed and course made good in the 3 hours preceding the report. We note that the radiative bias of the air temperature did not affect the accuracy of the reported dewpoint temperature (Kent and Taylor, 1996).

iv.) The reported values of wind speed (if based on anemometer readings), air temperature and humidity have been height corrected using the merged metadata from WMO47 for the cases where matching was successful. Default heights were applied where no information was available as follows: ships (anemometer height = 20m / temperature and humidity sensor height = 18m) , buoys (8 / 7m) and platforms (80 / 60m).

Many of the wind speed estimates reported in COADS1a, were obtained from visual observations of the sea state. These visual estimates are based on the WMO1100 Beaufort Equivalent Scale (WMO, 1970). The accuracy of this scale has often been questioned and many alternative scales suggested. Kent and Taylor (1997) compared ship based monthly mean wind speeds on a 1^{o} x 1^{o} grid. The Beaufort scale suggested recently by Lindau (1995) was found to give the best correspondence between winds from anemometers at known heights and the visual mean wind speeds; it has therefore been used in the present study.

3.2. Flux Formulae

Estimates of the heat flux components have been obtained for each report in the merged COADS1a / WMO47 dataset for which the relevant meteorological fields are available using the parameterisations described below.

3.2.1. Sensible and Latent Heat Fluxes

The sensible and latent heat fluxes, Q_H and Q_E, have been calculated using the bulk formulae

$$Q_H = \rho c_p C_h u (T_s - (T_a + \gamma z)) \quad (3)$$

$$Q_E = \rho L C_e u (q_s - q_a) \quad (4)$$

where ρ is the density of air; c_p, the specific heat capacity of air at constant pressure; L, the latent heat of vaporisation; C_h and C_e, the stability and height dependent transfer coefficients for sensible and latent heat respectively; u, the wind speed; T_s, the sea surface temperature ; T_a, the surface air temperature with a correction for the adiabatic lapse rate, γ; z, the height at which the air temperature was measured; q_s, 98% of the saturation specific humidity at the sea surface temperature to allow for the salinity of sea water, and q_a, the atmospheric specific humidity. The air density is determined from the ideal gas equation in the form,

$$\rho = 0.3484\, P / T_v \quad (5)$$

where the units of density are kgm^{-3}, P is the reported pressure in mb and T_v the virtual temperature. The formulae used for c_p and L have been taken from Stull (1988),

$$c_p = 1004.67 + 0.84 q_s \quad (6)$$

$$L = 10^6 [2.501 - 0.00237(T_s - 273.16)] \quad (7)$$

where the units are J $kg^{-1}K^{-1}$ for c_p and J kg^{-1} for L. The rate of evaporation, E, corresponding to the latent heat flux has also been determined by taking the ratio of Q_E to L.

Following Smith (1988) we have assumed neutral values for the sensible and latent heat flux transfer coefficients of 0.0010 and 0.0012 respectively. Stability dependent values have been calculated from these using the profile functions summarised in Smith (1988). A value for the neutral drag coefficient is also required for the heat flux calculations and for this we have used the wind speed dependent relationship of Smith (1980), which Yelland et al. (1998) have recently confirmed.

3.2.2. Wind Stress

Estimates of the zonal, τ_x, and meridional, τ_y, components of the wind stress has been determined using the bulk formula,

$$\tau_x = \rho C_D u_x (u_x^2 + u_y^2)^{1/2}$$
$$\tau_y = \rho C_D u_y (u_x^2 + u_y^2)^{1/2} \quad (8)$$

where C_D is a stability dependent drag coefficient, and u_x and u_y are the zonal and meridional components of the wind speed respectively. The neutral drag coefficient relationship of Smith (1980) has been employed for the calculations with stability dependent values being determined as noted above.

3.2.3. Longwave Flux

The performance of several bulk formula parameterisations for the net longwave flux has been assessed by comparison with radiometer measurements made at sea during a number of cruises (Josey et al., 1997). Results from this analysis show that the formula used by Clark et al. (1974) performs best under open ocean conditions in the North Atlantic and Southern Ocean giving estimates of the monthly mean longwave flux which are accurate to within 5 Wm^{-2}. The same analysis revealed that the longwave formula employed by Bunker (1976) tended to overestimate the downwelling longwave component and hence underestimate the net longwave loss from the ocean by of order 10 Wm^{-2} in the mean. The third formula considered was one suggested by Bignami et al. (1995), based on measurements in the Mediterranean Sea, an earlier version of which had been used in a budget analysis of that basin by Gilman and Garrett (1994). It was found to perform poorly under open ocean conditions, consistently overestimating the net oceanic longwave loss by 20 - 30 Wm^{-2}.

On the basis of this study we decided to employ the Clark formula, given below, to estimate the net longwave flux,

$$Q_{LW} = \varepsilon\sigma_{SB}T_s^4(0.39 - 0.05e^{1/2})(1 - \lambda n^2) + 4\varepsilon\sigma_{SB}T_s^3(T_s - T_a) \qquad (9)$$

where ε is the emittance of the sea surface, taken to be 0.98 ; σ_{SB}, the Stefan - Boltzmann constant, equal to 5.7 x 10^{-8} W m^{-2} K^{-4} ; e, the water vapour pressure; n, the fractional cloud cover; λ, a latitude dependent cloud cover coefficient; T_s and T_a , the sea surface and air temperatures in degrees Kelvin.

3.2.4. Shortwave Flux

The monthly mean net shortwave flux, $\overline{Q}_{SW}$, has been determined using the Reed (1977) formula which is based on an analysis of weather ship and coastal station measurements,

$$\overline{Q}_{SW} = (1-\alpha)Q_c[1 - 0.62\,\overline{n} + 0.0019\,\overline{\theta}_N] \qquad (10)$$

where α is the albedo ; Q_c, the clear - sky solar radiation ; $\overline{n}$, the monthly mean fractional cloud cover and $\overline{\theta}_N$, the monthly mean local noon solar elevation. Note that in this case we have employed a monthly mean flux formula rather than obtaining individual estimates as there is a

significant diurnal bias in the number of reports within COADS1a which would give rise to a bias in the mean shortwave flux if a simple average were taken over the individual values. Values for α were taken from Payne (1972), for Q_c we have made use of the formulation suggested by Seckel and Beaudry (1973) which Reed originally employed, while $\overline{\theta}_N$ is an average over all daily values in the month determined using formulae summarised in Reed (1977). Gilman and Garrett (1994) note that under conditions of low cloud cover the Reed formula estimate of the mean incoming shortwave can become greater than the clear-sky value if $\overline{\theta}_N$ is sufficiently large. We follow their suggestion that the incoming shortwave be constrained to be less than or equal to Q_c.

Although not employed to calculate the monthly mean, instantaneous shortwave estimates were used for the radiation correction to the air temperature (see 3.1.) using the 'okta' model of Dobson and Smith (1988),

$$Q_{SW} = (1-\alpha) Q_o \sin\theta (A_i + B_i \sin\theta) \qquad (11)$$

where Q_o is the solar constant taken to be 1368 Wm^{-2} (Frohlich and London, 1986); A_i and B_i, empirically determined coefficients for each category of reported total cloud amount in oktas and θ, the solar elevation.

3.2.5. Net Heat Flux

The net heat flux, Q_{Net}, is given by the sum of the four individual components,

$$Q_{Net} = Q_H + Q_E + Q_{LW} + \overline{Q}_{SW} \qquad (12)$$

Note that the sign convention followed in the maps presented later in this atlas is for positive fluxes to represent a heat gain by the ocean.

3.2.6. Precipitation

Estimates of the precipitation rate, P, have been obtained for each report from the Present Weather field where available in COADS1a using a modified version of the empirical parameterisation developed by Tucker (1961). The parameterisation was originally based on station data collected in the vicinity of the British Isles and has subsequently been revised by Dorman and Bourke (1978) in an attempt to allow for the stronger rainfall rates typical of the tropics. For this purpose, they introduced an air temperature dependent correction factor and we have made use of their suggested annual mean relationship such that,

$$P = (a + bT_a + cT_a^2) P_T \qquad (13)$$

where P_T is the rate obtained with original Tucker (1961) parameterisation, a= 0.507, b= 0.0506 and c= 0.00341.

3.3. Generation of Climatological Means

Outliers were removed from the set of individual flux estimates prior to calculating gridded mean flux fields using the 4.5 σ trimming flags that are included within COADS1a for the zonal and meridional wind speed, sea surface and air temperatures, humidity and sea level pressure. For this purpose a flux estimate was removed from the subsequent analysis if the trimming flags indicated that any of the variables on which it depended lay outside the 4.5 σ limits. Raw mean flux fields were generated from the resulting trimmed dataset by averaging over individual reports for each month in the period January 1980 - December 1993 on a 1^{o} x 1^{o} grid spanning the region 85^{o} N - 85^{o} S. This approach (commonly termed the sampling approach) has been taken rather than calculating fluxes from monthly averaged meteorological variables (the classical approach). In an earlier study, using data from a weather ship in the North Atlantic (Josey et al., 1995), we found that the estimated heat loss may be biased high by of order 10% if classical means are used due to the effects of correlations between meteorological variables, particularly wind speed and humidity, which are neglected when taking classical means. The sign and magnitude of such biases are likely to vary with region depending on variations in the correlation fields of the various meteorological variables ; see Hasse and Smith (1997) for a review of sampling / classical comparisons in other regions.

It is important to remember that the distribution of ship reports and hence of the estimated fluxes shows strong spatial variations with the data being concentrated in the North Atlantic and North Pacific and falling away sharply in the Southern Hemisphere. As an example, the number of latent heat flux estimates per 1^{o} x 1^{o} square used to form the climatological monthly mean, averaged over all months of the year, is shown in Figure 2. In the mid-latitude Northern Hemisphere oceans there are typically greater than 10 observations per 1^{o} x 1^{o} square with greater than 100 in the heavily sampled regions. However, large areas with very few or no observations are evident in the Southern Hemisphere particularly in the austral winter.

In past analyses, various approaches have been taken to the problem of non-uniformity in the ship distribution ranging from increasing the size of the grid cells in data sparse areas (Bunker, 1976) to more complex objective analysis procedures (e.g. da Silva et al., 1994) which aim to produce estimates for the unsampled regions of a grid in addition to smoothing out extreme values. We have chosen a technique similar to that employed by da Silva et al. (1994) which in turn was based on one used in an earlier analysis of sub-surface data by Levitus (1982). The scheme is a successive correction method (SCM) of the type developed by Cressman (1959), in which the analysed field at a particular point is given by the sum of a background field at that point and the weighted mean of the differences between all observed values within a specified radius of influence and the background field at their respective locations. The analysis is repeated several times with the background field for each iteration being provided by the analysed field

from the previous one and the radius of influence being reduced on each pass in order to restore information at successively smaller scales.

Defining $X^{a(k)}$ to be the value of the analysed field at a particular location on the k^{th} pass then the corresponding value on the following pass is given by,

$$X^{a(k+1)} = X^{a(k)} + \sum h_j^{(k+1)}(X_j^o - X_j^{a(k)}) \qquad (14)$$

where the sum is over all grid points for which there are observations (i.e. raw mean values in the analysis treated here) within a region of influence of radius, R, about the analysed point, and X_j^o and $X_j^{a(k)}$ are the observed value and the analysed value on the k^{th} scan at each grid point. On the first pass the background, $X^{a(0)}$, is given by an appropriate first-guess field, a zonal average in the case of Levitus (1982). The weight function, $h_j^{(k+1)}$, contains a dependence on the distance of each observation from the analysed point via a Gaussian function of the type suggested by Barnes (1964),

$$\begin{aligned} h_j(r_j) &= \frac{\exp(-4r_j^2/R^2)}{\sum \exp(-4r_j^2/R^2)} \quad , \quad r_j \le R \\ &= 0 \qquad\qquad\qquad , \quad \text{otherwise} \end{aligned} \qquad (15)$$

where r_j is the distance of the j^{th} grid point from the point to be analysed and the sum is again over all grid points with observations within the radius of influence. In our analysis, each individual monthly raw mean field has been analysed using the above technique with four passes at influence radii of 1541, 1211, 771 and 331 km respectively and a zonal mean field as a first guess. We have chosen to use 331 km as the minimum influence radius as opposed to the value of 771 km adopted by da Silva et al. (1994) as test studies indicated that it provides a better definition of frontal features, e.g. the Gulf Stream, in well sampled areas. We are aware that such a choice can lead to 'bullseye' features in data sparse areas. However, we have not attempted to increase the minimum radius in such regions as we want to avoid changes in the characteristic scale of features that span both well sampled and data sparse areas. Note that climatologically ice covered regions were excluded from the objective analysis using the monthly mean ice mask of Alexander and Mobley (1976).

The analysed fields are smoothed after each pass with a combination of non-linear and linear filters following the approach of da Silva et al. (1994). A non-linear filter is first used to generate a smoothed value which is the median of the nine points in a 3^o x 3^o cell centred on the point concerned. This is followed by two passes of a linear filter (Shapiro, 1970) for which if $X_{i,j}^{NL}$ denotes the field value at grid point (i , j) after the application of the non-linear filter, the linear filtered value is,

$$X_{i,j}^{L} = X_{i,j}^{NL} + \frac{\alpha}{4}(X_{i-1,j}^{NL} + X_{i+1,j}^{NL} + X_{i,j-1}^{NL} + X_{i,j+1}^{NL}) \qquad (16)$$

On the first pass, the smoothing parameter α=0.5 and on the second -0.5. The resulting smoothed fields provide the background for the next pass of the SCM.

The climatological monthly mean fields were generated from the individual monthly analysed fields produced according to the above method for the period 1980-93.

3.4. Estimation of Random Errors

Estimation of the random errors in ship-based climatological flux fields requires knowledge of the errors inherent in the original meteorological observations, of the strength of the spatial and temporal correlations between the variables in the flux formulae, and of the propagation of errors during the objective analysis. Gleckler and Weare (1997) have recently attempted to estimate the errors in the Oberhuber (1988) flux climatology using estimates for the random errors and standard sampling theory. Following the method of Lindau (1995), Kent et al. (1998) have determined the random errors in the meteorological observations used in calculating the SOC climatology. However, at present we do not consider our knowledge of the many meteorological variable correlation terms sufficient to use their results to derive error fields for the climatology. An assessment of the overall accuracy of the calculated flux values has been made by Josey et al. (1999) using comparisons with local flux estimates from research buoy deployments and regional flux estimates obtained from hydrography.

4. Field Characteristics

4.1. Climatological Mean Fields

In this section we give an overview of the main characteristics of the flux fields, presenting climatological mean maps and summary plots of the global zonal mean variation in each field for January, April, July and October. The climatological mean flux fields are shown in Figs. 3 - 10 and the corresponding zonal mean variation in each in Fig. 11. We stress that caution must be exercised when interpreting the fields in data sparse areas, particularly south of 40^{o} S.

4.1.1. Latent Heat Flux

The pattern of latent heat loss is primarily determined by a combination of the wind speed and sea - air humidity difference. The strongest losses, of order -250 Wm^{-2}, are found over the Gulf Stream and Kuroshio in January. Enhanced heat loss is also seen over the Agulhas and East Australian currents in the austral winter but these regions are somewhat weaker than their

Northern Hemisphere counterparts. Broader areas of less intense heat loss are observed under the main trade wind belts in winter, particularly in the Southern Indian Ocean in July; the wind field in this region is stronger than at corresponding latitudes in the South Atlantic and South Pacific. The trade wind related losses give rise to the strongest signal in the zonal mean variation with peak values of order -140 Wm^{-2}.

4.1.2. Sensible Heat Flux

The sensible heat flux field also exhibits strong losses, typically -100 Wm^{-2}, over the western boundary currents due to the large sea - air temperature difference. In contrast to the latent heat, intense sensible heat loss is observed at high northern latitudes in regions where very cold air is advected over the ocean from neighbouring land masses, particularly the Labrador and Norwegian Seas as noted by Bunker (1976). Note, that the true northward extent of these regions is probably underestimated in our analysis as we have not been able to include heat loss through leads in regions covered by the climatological ice mask. Elsewhere, the field is relatively uniform and significantly weaker than the latent, with typical values being of order -10 Wm^{-2}.

4.1.3. Longwave Flux

The global variation in the longwave flux is relatively small, typically ranging from -30 to -70 Wm^{-2}. However, within this range there is a degree of structure which reflects the balance between the sea - air temperature difference, the cloud cover and the amount of water vapour in determining the net longwave flux. Noticeable features include the bands of reduced longwave loss under the Inter - Tropical and South Pacific Convergence Zones (ITCZ and SPCZ), while maxima occur over the Western Boundary Currents in winter where the sea-air temperature difference is high. The zonal mean variation shows a seasonal shift in the band of enhanced longwave loss in the sub-tropics either side of the equator; the strongest losses, about -60 Wm^{-2}, occurring in the Winter Hemisphere.

4.1.4. Shortwave Flux

The shortwave field has a primarily meridional variation determined by the mean solar elevation with peak summer values of order 350 Wm^{-2} locally, falling to 250 Wm^{-2} in the zonal mean. The main departures from this variation occur under regions of increased cloud cover such as the ITCZ and SPCZ. The position of the ITCZ is evident in the zonal mean variation as a local minimum just north of the Equator.

4.1.5. Net Heat Flux

The net heat flux field is largely determined by the opposing contributions from the shortwave and latent heat fluxes with heat gain primarily confined to the Summer Hemisphere and heat loss to the Winter. Over the Northern Hemisphere western boundary currents the net heat loss reaches -350 Wm^{-2} in winter. The strongest gains, of order 250 Wm^{-2} are found in the Mediterranean Sea in summer.

4.1.6. Wind Stress

The SOC wind stress fields are in broad agreement with those obtained by Hellerman and Rosenstein (1983) in terms of the main features, although the magnitude of the stresses is typically weaker due to our use of the Smith (1980) drag coefficient scheme. Comparisons to be reported in a future paper indicate that the main difference is to be found in the mid-latitude North Pacific in January, a single basin-wide cyclonic gyre being found in the SOC analysis in contrast to the two gyre structure of Hellerman and Rosenstein (1983). The difference probably reflects variations arising from the different time periods sampled in each analysis. The greatest zonal mean stresses are found in the Southern Ocean with τ_x values in the range 0.1-0.18 Nm^{-2}.

4.1.7. Precipitation

The precipitation fields clearly show the bands of enhanced rainfall expected under the ITCZ and SPCZ. These features dominate the global field, with secondary areas of significant rainfall occurring along the main storm track paths in the North Pacific and North Atlantic. The northward movement of the ITCZ between January and July is evident in the zonal mean plot. and the peak zonal mean precipitation increases from 160 to 230 mm $month^{-1}$ over the same period, reflecting the extra contribution associated with the Asian monsoon in summer.

4.1.8. Net Evaporation, E - P

The primary variation in the net evaporation field is that between the trade wind belts, where the broad band of significant latent heat loss and minimal rainfall lead to strong evaporative losses, and the two convergence zones, in which the high precipitation rates lead to a net gain of freshwater by the ocean. This variation is most evident in the zonal mean E - P, which reaches 100 mm $month^{-1}$ in both the Northern and Southern Hemisphere trade wind zones in winter, compared with values as low as -125 mm $month^{-1}$ along the ITCZ.

5. Estimation of Systematic Errors Due to Observing Procedure

In this section, we attempt to quantify the systematic errors in the flux fields due to variations in observation procedure that we have been able to correct for as described in 3.1. Ideally we would like to compare climatological mean fields obtained with and without each of the corrections. However, given the amount of additional time that would be required to produce parallel climatologies with each of the various corrections, we have restricted our comparison to the raw mean fields obtained for alternate months in 1990 and present results for January and July of that year. We expect these results to be broadly applicable to the climatological mean fields.

We have calculated an 'uncorrected' set of fluxes using the reported meteorological fields in COADS1a without the various bias corrections (using platform default heights for the instruments) and compared them with the corresponding fields obtained with each of the corrections applied individually and with the fields obtained with the full set of corrections. Note that the corrections do not affect the shortwave radiation. We first discuss the impact of the corrections at an individual level and then show plots of the changes that arise from their combined application to the latent, sensible, longwave and net heat flux fields.

5.1. Effect of Individual Corrections

The reduction in engine intake measured SST acted to lower both the sensible and latent heat loss, the latter as a result of the reduction in the specific humidity at the sea surface. The effect on the sensible heat was largest, up to 4 Wm^{-2}, in the northern North Pacific in January. The reduction in latent heat flux loss was strongest in the mid-latitude and Equatorial Pacific reaching over 10 Wm^{-2} in January. The SST correction also acted to decrease the net longwave cooling due to the reduction in the upwelling component. Changes were generally small, of order 1 Wm^{-2}, reaching a maximum of 2 Wm^{-2} in the Western North Pacific.

In contrast, the reduction of the air temperature resulting from the radiation correction, ΔT_{rad}, acted to increase the sensible heat and net longwave loss. The effect on each of these components was strongly seasonal and zonal with changes up to 5 Wm^{-2}. ΔT_{rad} also had an influence via the stability on the estimated latent heat flux. Changes due to this effect were small over much of the ocean, however, the heat loss was increased locally by up to 3 Wm^{-2} in the Indian Ocean and Equatorial regions.

The reduction to screen measured dewpoint temperatures served to increase the latent heat loss. This correction had the greatest effect over the Atlantic where there is a higher proportion of ships using screens than in the Pacific. Over most of the Atlantic the increase was greater than 4 Wm^{-2} with peak values of about 10 Wm^{-2}. As would be expected, the effect of the changes to the

latent heat flux is greater in winter than in the summer. Changes in the net longwave and sensible heat flux due to the dewpoint correction were negligible.

The use of the Lindau scale and individual anemometer heights affected the latent and sensible heat fluxes as a result of changes in the estimated wind speed. With the Lindau scale visual wind speed estimates of less than 11 ms^{-1} were increased relative to the WMO1100 scale values by about 0.3 - 0.4 ms^{-1}. At higher wind speeds the scale acted to progressively reduce the original values e.g. by 1 ms^{-1} at 15.5 ms^{-1} and by 3 ms^{-1} at 26 ms^{-1}. The combined effect on the turbulent fluxes was complex depending on changes in the ratio of visual to measured wind speed estimates between basins. In the Atlantic, visual wind estimates dominate with the consequence that the turbulent fluxes were reduced in regions of high wind speed i.e. the Central North Atlantic in January and increased in regions of low wind speed e.g. much of the Atlantic in July, the magnitude of the changes being up to 2 and 8 Wm^{-2} respectively. In the Pacific, anemometers rather than visual observations were the dominant source of wind speed values. Mean anemometer heights were found to be higher than in the Atlantic, typically greater than 30 metres, and the major change in the turbulent fluxes in the North Pacific was a reduction of order 10 Wm^{-2} in the latent heat flux due to the reduced wind speed.

5.2. Combined Effect of the Corrections

We now consider the combined effects of the corrections described above on each of the flux components and the net heat flux. Plots of the difference between the fully corrected and uncorrected flux fields for January and July 1990 are shown in Fig. 11, while summary statistics for certain key regions are listed in Table 1. Positive values indicate an increased heat loss by the ocean as a result of the corrections.

The combined effect of the corrections on the sensible heat loss was similar in both the Atlantic and the Pacific. In January, the SST correction dominated in the northern latitudes and the sensible heat loss was reduced by up to 4 Wm^{-2}. Further south the ΔT_{rad} correction became important and in the tropics the heat loss was increased by a similar amount. In July, increases in sensible heat loss of order 2 Wm^{-2} were observed in most regions due to ΔT_{rad} (see Table 1). However, at the very southern limit of the data coverage the effect of the SST correction still dominated and small reductions were found. The latent heat loss in January was increased by up to 8 Wm^{-2} in the Southern Hemisphere, the Indian Ocean, and Tropical North Atlantic due to the humidity correction. In contrast over most of the North Pacific and the Gulf Stream region reductions of up to 10 Wm^{-2} were found as the effects of the anemometer heights corrections and use of the Lindau scale were dominant. The area of strong reduction noted in the North Pacific was significantly smaller in July. For the longwave flux, the January distribution of flux change showed a mainly zonal pattern due to the ΔT_{rad} correction with the largest increases, above 4

Wm^{-2}, in the Southern Hemisphere mid-latitudes. The situation was reversed in July with the effects of ΔT_{rad} shifted towards the Northern Hemisphere.

The combined effect of the corrections on the net heat flux, or equivalently the systematic error in an uncorrected heat flux field due to observational bias, has a complex spatial variation. In January increases in the heat loss of up to 15 Wm^{-2} are seen in the Southern Hemisphere (driven mainly by changes in the latent heat flux) while reduced loss is seen in the Northern Hemisphere. In July the situation is reversed in the northern oceans with increased heat loss occurring; further south the heat loss also tended to increase as a result of the corrections but by a smaller amount than in January. Finally note that there was reduced heat loss at the limit of data coverage in the South where the SST correction started to become important.

6. Conclusion

In this atlas we have presented a new set of climatological air-sea flux fields developed at the Southampton Oceanography Centre (SOC). The method by which the fluxes were calculated has been documented in detail and an overview of the main characteristics of the climatological monthly mean fields given. The climatology was generated by applying empirical flux formulae to surface meteorological reports in the COADS1a merged with additional metadata from the WMO47 list of ships. The additional metadata have allowed corrections to be made to the meteorological variables for biases arising from observational procedure. The effect of the corrections is complex, and we have attempted to quantify it by calculating repeat fields for sample months in which various subsets of the corrections are made. Regional changes of up to 15 Wm^{-2} are found with significant seasonal variations depending primarily on the spatial distribution of different measurement methods and incident solar radiation as well as the magnitude of the flux component being corrected.

In a separate study (Josey et al., 1999), the accuracy of the individual monthly flux fields has been assessed using high quality research buoy measurements at several climatically different locations. In addition, regional mean surface heat fluxes derived from hydrographic section data have been compared with the corresponding SOC values giving further insight into regional biases within the climatology. The results of that analysis indicate that although closure of the ocean heat budget is not obtained with the SOC fields, the imbalance of 30 Wm^{-2} that is found appears to be due to various regionally dependent processes rather than to systematic global biases. These processes are separate from the various biases due to observing procedure discussed above. When globally averaged, the latter corrections tend to cancel out and they do not have a significant impact on the global mean heat flux.

Comparisons with hydrography potentially provide a method to correct the fields on a regional basis. However, at present we are limited by the area of ocean bound by reliable hydrographic estimates of the heat transport and so have not attempted to produce an adjusted set of flux fields for which the heat budget is closed. As more hydrographic estimates become available in the future we envisage being able to produce a regionally adjusted version of the SOC flux climatology in which the global heat budget is closed without the introduction of biases in regions that do not require adjustment.

Acknowledgements

The preparation of the SOC flux climatology was partially funded by a commissioned research project for the Hadley Centre, UK Meteorological Office. The authors would like to thank Steven Worley at the Data Support Section, NCAR and Scott Woodruff at the NOAA / ERL Climate Diagnostics Center for supplying the COADS 1a ; Arlindo da Silva at the Data Assimilation Office, NASA/GSFC for advice and providing the objective analysis code and Daniel Oakley formerly at SOC for assistance in preparing the merged COADS1a / WMO47 dataset.

Availability of Fields: The SOC flux climatology is freely available to interested users for non-commercial scientific research, for details of how to access the fields see http://www.soc.soton.ac.uk/JRD/MET/fluxclimatology.html

References

Alexander, R. and R. Mobley, 1976: Monthly average sea-surface temperature and ice-pack limits on a 1 degree global grid. Mon. Wea. Rev., **104**, 143 - 148.

Barnes, S. L., 1964: A technique for maximizing details in numerical weather map analysis. J. App. Meteor., **3**, 396 - 409.

Berliand, M. E. and T. G. Berliand, 1952: Measurements of the effective radiation of the earth with varying cloud amounts (in Russian). Izv. Akad. Nauk SSSR Ser. Geofiz., 1.

Bignami, F., S. Marullo, R. Santoleri and M. E. Schiano, 1995: Longwave radiation budget in the Mediterranean Sea. J. Geophys. Res., **100**(C2), 2501 - 2514.

Budyko, M. I., 1963: Atlas of the heat balance of the earth. Kartfabrika Gosgeoltehiydata, 41pp.

Bunker, A. F., 1976: Computations of surface energy flux and annual air-sea interaction cycles of the North Atlantic Ocean. Mon. Wea. Rev., **104**, 1122-1140.

Businger, J. A., 1973: Turbulent transfer in the atmospheric surface layer. Workshop on Micrometeorology, D. A. Haugen, Ed., American Meteorological Society, 67 - 100.

Clark, N. E., L. Eber, R. M. Laurs, J. A. Renner and J. F. T. Saur, 1974: Heat exchange between ocean and atmosphere in the eastern North Pacific for 1961 - 71. NOAA Tech. Rep. NMFS SSRF-682, U.S. Dept. of Commer., Washington, D.C, 108 pp.

Cressman, G. P., 1959: An operational objective analysis scheme. Mon. Wea. Rev., **87**, 329 - 340.

da Silva, A. M., C. C. Young and S. Levitus, 1994: Atlas of Surface Marine Data Vol. 1: Algorithms and Procedures. NOAA Atlas series, 74 pp.

Dobson, F. W. and S. D. Smith, 1988: Bulk models of solar radiation at sea. Q. J. R. Meteorol. Soc., **114**, 165 - 182.

Dorman, C. E. and R. H. Bourke, 1978: A temperature correction for Tucker's ocean rainfall estimates. Q. J. Royal Meteor. Soc., **104**, 765 - 773.

Dyer, A. J., 1974: A review of flux-profile relationships. Boundary Layer Meteorol., **7**, 363 - 372.

Esbensen, S. K. and Y. Kushnir, 1981: The heat budget of the global ocean: an atlas based on estimates from surface marine observations. Climate Research Institute Report No. 29, Oregon State University, 244 pp.

Frohlich, C. and J. London, 1986: Revised instruction manual on radiation instruments and measurements. *WCRP Pub. Ser. 7* , WMO, Geneva, 74 pp.

Gilman, C. and C. Garrett, 1994: Heat flux parameterizations for the Mediterranean Sea : The role of atmospheric aerosols and constraints from the water budget. Journal of Geophysical Research, **99**(C3), 5119 - 5134.

Gleckler, P. J. and B. C. Weare, 1997: Uncertainties in global ocean surface heat flux climatologies derived from ship observations. J. Clim., **10**(11), 2764 - 2781.

Hasse, L. and S. D. Smith, 1997: Local sea surface wind, wind stress, and sensible and latent heat fluxes. J. Clim., **10**(11), 2711 - 2724.

Hellerman, S. and M. Rosenstein, 1983: Normal monthly wind stress over the World Ocean with error estimates. J. Phys. Oceanogr., **13**, 1093 - 1104.

Hsiung, J., 1986: Mean surface energy fluxes over the global ocean. J. Geophys. Res., **91**(C9), 10585-10606.

Isemer, H.-J. and L. Hasse, 1987: The Bunker climate atlas of the North Atlantic Ocean. Vol.2: Air-sea interactions. Springer-Verlag, 252 pp.

Josey, S. A., E. C. Kent and P. K. Taylor, 1995: Seasonal variations between sampling and classical mean turbulent heat flux estimates in the eastern North Atlantic. Annales Geophysicae, **13**, 1054 - 1064.

Josey, S. A., E. C. Kent and P. K. Taylor, 1999: New insights into the ocean heat budget closure problem from analysis of the SOC air-sea flux climatology. Journal of Climate, submitted.

Josey, S. A., D. Oakley and R. W. Pascal, 1997: On estimating the atmospheric longwave flux at the ocean surface from ship meteorological reports. Journal of Geophysical Research, **102**(C13), 27,961 - 27,972.

Katsaros, K. B., 1990: Parameterization schemes and models for estimating the surface radiation budget. Surface Waves and Fluxes: Volume II - Remote Sensing, ed., G. L. Geernaert and W. J. Plant, Kluwer Academic Publishers, 339-368.

Kent, E. C. and P. K. Taylor, 1991: Ships observing marine climate: A catalogue of the voluntary observing ships participating in the VSOP-NA. World Meteorological Organisation, Marine Meteorology and Related Oceanographic Activities Report No 25, 123 pp.

Kent, E. C. and P. K. Taylor, 1995: A comparison of sensible and latent heat flux estimates for the North Atlantic Ocean. J. Phys. Oceanogr., **25**(6), 1530 - 1549.

Kent, E. C. and P. K. Taylor, 1996: Accuracy of humidity measurements on ships: Consideration of solar radiation effects. J. Atmos. & Oceanic Tech., **13**(6), 1317-1321.

Kent, E. C. and P. K. Taylor, 1997: Choice of a Beaufort Equivalent Scale. J. Atmos. & Oceanic Tech., **14**(2), 228-242.

Kent, E. C., P. G. Challenor and P. K. Taylor, 1998: A statistical determination of the random errors present in voluntary observing ships meteorological reports. J. Atmos. Ocean. Tech., accepted.

Kent, E. C., P. K. Taylor, B. S. Truscott and J. A. Hopkins, 1991: The accuracy of ship's meteorological observations - Results of the VSOP-NA. World Meteorological Organisation, Marine Meteorology and Related Oceanographic Activities Report No 26, 86 pp.

Kent, E. C., P. K. Taylor, B. S. Truscott and J. S. Hopkins, 1993a: The accuracy of voluntary observing ships meteorological observations - results of the VSOP - NA. J. Atmos. & Oceanic Tech., **10(4)**, 591 - 608.

Kent, E. C., R. J. Tiddy and P. K. Taylor, 1993b: Correction of marine air temperature observations for solar radiation effects. J. Atmos. & Oceanic Tech., **10(6)**, 900 - 906.

Levitus, S., 1982: Climatological Atlas of the World Ocean. NOAA Prof. Paper No. 13, US Government Printing Office, Washington DC, 17 fiches, 173 pp.

Lindau, R., 1995: A new Beaufort equivalent scale. *International COADS Winds Workshop*, June 1994, Kiel, 232 - 252.

Oberhuber, J. M., 1988: An atlas based on the COADS data set : the budgets of heat, buoyancy and turbulent kinetic energy at the surface of the global ocean. MPI Report, **15**.

Paulson, C. A., 1970: The mathematical representation of wind speed and temperature profiles in the unstable atmospheric surface layer. J. Appl. Meteorol., **9**, 857 - 861.

Payne, R. E., 1972: Albedo of the sea surface. J. Atmos. Sci., **29**, 959 - 970.

Reed, R. K., 1977: On estimating insolation over the ocean. J. Phys. Oceanogr., **7**, 482-485.

Schulz, J., J. Meywerk, S. Ewald and P. Schlussel, 1997: Evaluation of satellite derived latent heat fluxes. J. Clim., **10**(11), 2782 - 2795.

Seckel, G. R. and F. H. Beaudry, 1973: The radiation from sun & sky over the Pacific Ocean (Abstract). Trans. Amer. Geophys. Union, **54**, 1114.

Shapiro, R., 1970: Smoothing, filtering and boundary effects. Rev. of Geophys. and Space Phys., **8**, 359 - 387.

Smith, S. D., 1980: Wind Stress and Heat Flux over the Ocean in Gale Force Winds. J. Phys. Oceanogr., **10**, 709-726.

Smith, S. D., 1988: Coefficients for sea surface wind stress, heat flux and wind profiles as a function of wind speed and temperature. J. Geophys. Res., **93**, 15467-15474.

Stull, R. B., 1988: An Introduction to Boundary Layer Meteorology. Kluwer Academic Publishers, 666 pp.

Tucker, G. B., 1961: Precipitation over the North Atlantic Ocean. Q. J. Royal Meteor. Soc., **87**, 147 - 158.

WCRP, 1986: Scientific Plan for the World Ocean Experiment. WCRP Publications Series No.6 , WMO/TD No.122, 83 pp.

WCRP/GEWEX, 1996: Report of the eighth session of the working group on radiative fluxes. WCRP Informal Report No.13/1996, Killiney Bay, Dublin, Ireland, 22-26 July 1996.

WMO, 1970: The Beaufort Scale of Wind Force (Technical and Operational Aspects). World Meteorological Organisation Reports on Marine Science Affairs. Report No 3, 22 pp.

WMO, 1993: International list of selected, supplementary and auxiliary ships. WMO Report, WMO, Geneva, various pagination.

Woodruff, S. D., S. J. Lubker, K. Wolter, S. J. Worley and J. D. Elms, 1993: Comprehensive Ocean-Atmosphere Data Set (COADS) release 1a: 1980-92. Earth System Monitor, **4**(1), 4-8.

Woodruff, S. D., R. J. Slutz, R. L. Jenne and P. M. Steurer, 1987: A comprehensive ocean-atmosphere data set. Bull. Amer. Met. Soc., **68**(10), 1239-1250.

Yelland, M. J., B. I. Moat, P. K. Taylor, R. W. Pascal, J. Hutchings and V. C. Cornell, 1998: Wind stress measurements from the open ocean corrected for air flow disturbance by the ship. J. Phys. Oceanogr., **28**(7), 1511-1526.

Tables

Region	Month	Sensible		Latent		Longwave		Net
Mid Pacific	Jan	0.3		-3.2	S, I	0.7	R	-2.2
15 - 25N; 180 - 150W	Jul	0.8		-0.8		2.8		2.8
Gulf Stream	Jan	-		0.8	H	0.4	R	1.2
35 - 45N; 70 - 60W	Jul	1.0		2.5	R, H	3.0	R	6.5
Mid North Atlantic	Jan	-		2.1	H, I	0.8		2.9
30 - 40N; 40 - 30W	Jul	2.6	R	6.1	R	4.1	R, H, I	12.8
Tropical Atlantic	Jan	2.6	R	5.4	H, I	3.0	R	11.0
5S - 10N; 50W - 0E	Jul	3.0	R	5.5	R, H, I	3.2	R	11.7
Atlantic High Latitudes	Jan	-1.2	S, I	4.5	H	0.3		3.6
55 - 80N; 20W - 40 E	Jul	1.1	R	3.8	H	2.1	R	7.0
Tropical Pacific	Jan	1.6	R	-		1.7	R	3.3
10S - 10N; 100 - 160 E	Jul	1.5	R	-		1.8	R	3.3
Kuroshio	Jan	-1.8	S	-4.4	S, I	-		-6.2
30 - 40N; 140 - 150E	Jul	1.1	R	-1.7	S	1.1	R	0.5

Table 1 - Regional Effect of the VSOP-NA Corrections, units Wm^{-2}, positive values indicate an increase in heat loss by the ocean following the corrections. For the sensible, latent and longwave fluxes the dominant corrections are indicated as follows: 'S' for the SST correction ; 'I' for the combined effects of the individual height correction and the Lindau Scale; 'R', for the radiation correction to air temperature and 'H' for the screen dewpoint correction.

Figures

Figure 1) Time series of the total number of reports, N(reports), for each individual month over the period January 1980 - December 1993 in the filtered version of COADS1a , i.e. that in which reports with the source exclusion flag set have been removed ; the number of those which are ship reports, N(ships), and the number of reports for which matching has been possible with an entry in the WMO47 list of ships N(matched).

Figure 2) Global distribution of the total number of latent heat flux estimates available to generate a climatological mean (averaged over all months of the year) per 1^{o} x 1^{o} square for the period 1980-93. White indicates that there were no observations over the entire period considered.

Figure 3) Climatological mean latent heat flux field for a.) January ; b.) April ; c.) July and d.) October. Units Wm^{-2}.

Figure 4) Climatological mean sensible heat flux field for a.) January ; b.) April ; c.) July and d.) October. Units Wm^{-2}.

Figure 5) Climatological mean longwave flux field for a.) January ; b.) April ; c.) July and d.) October. Units Wm^{-2}.

Figure 6) Climatological mean shortwave flux field for a.) January ; b.) April ; c.) July and d.) October. Units Wm^{-2}.

Figure 7) Climatological mean net heat flux field for a.) January ; b.) April ; c.) July and d.) October. Units Wm^{-2}.

Figure 8) Climatological mean wind stress field for a.) January ; b.) April ; c.) July and d.) October. Units Nm^{-2}.

Figure 9) Climatological mean precipitation field for a.) January ; b.) April ; c.) July and d.) October. Units mm $month^{-1}$.

Figure 10) Climatological mean net evaporation field for a.) January ; b.) April ; c.) July and d.) October. Units mm $month^{-1}$.

Figure 11) Global zonal means of a.) latent ; b.) sensible ; c.) longwave ; d.) shortwave ; e.) net heat ; f.) eastward wind stress ; g.) northward wind stress ; h.) vector mean wind stress magnitude; i.) precipitation and j.) net evaporation. Solid line (January) ; dash-dot (April) ; long dash (July) and dotted (October).

Figure 12) Global distribution of the difference between the fully corrected and uncorrected flux fields for January and July 1990: a-b) sensible; c-d) latent ; e-f) longwave and g-h) net heat flux. Units Wm^{-2}.

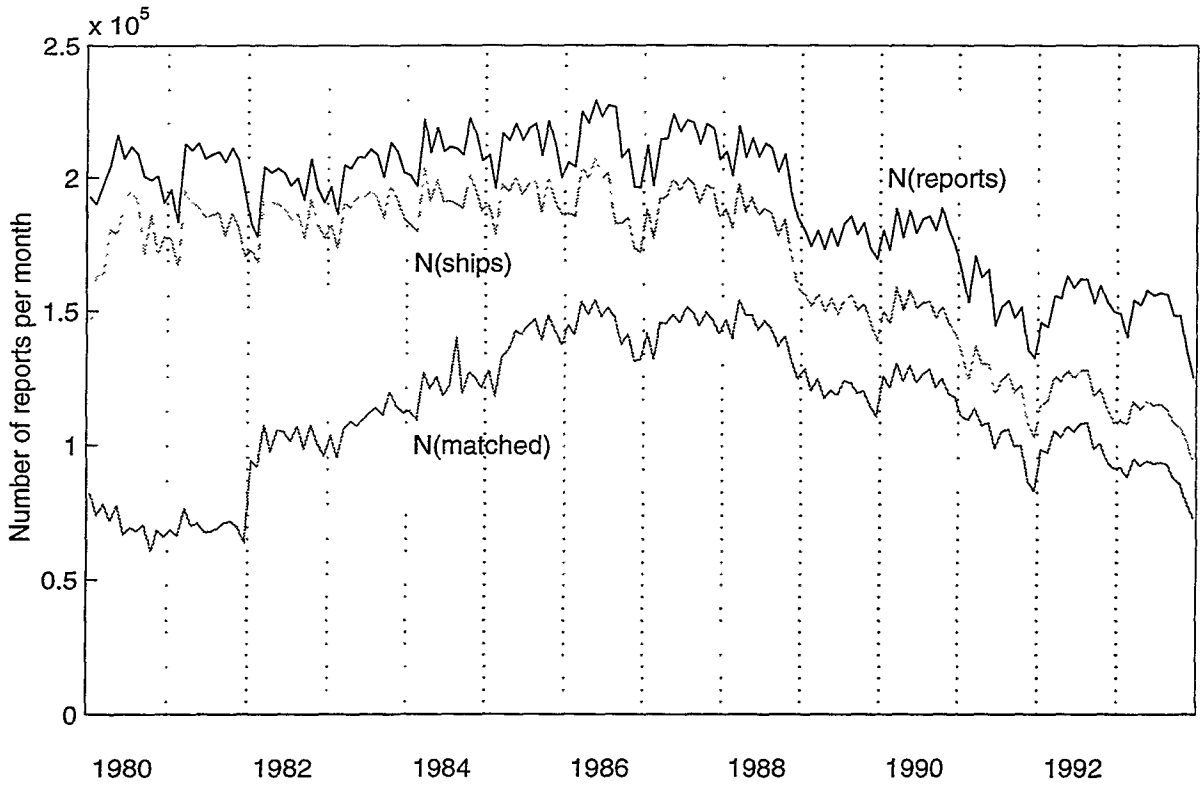

Figure 1) Time series of the total number of reports, N(reports), for each individual month over the period January 1980 – December 1993 in the filtered version of COADS1a , i.e. that in which reports with the source exclusion flag set have been removed ; the number of those which are ship reports, N(ships), and the number of reports for which matching has been possible with an entry in the WMO47 list of ships N(matched).

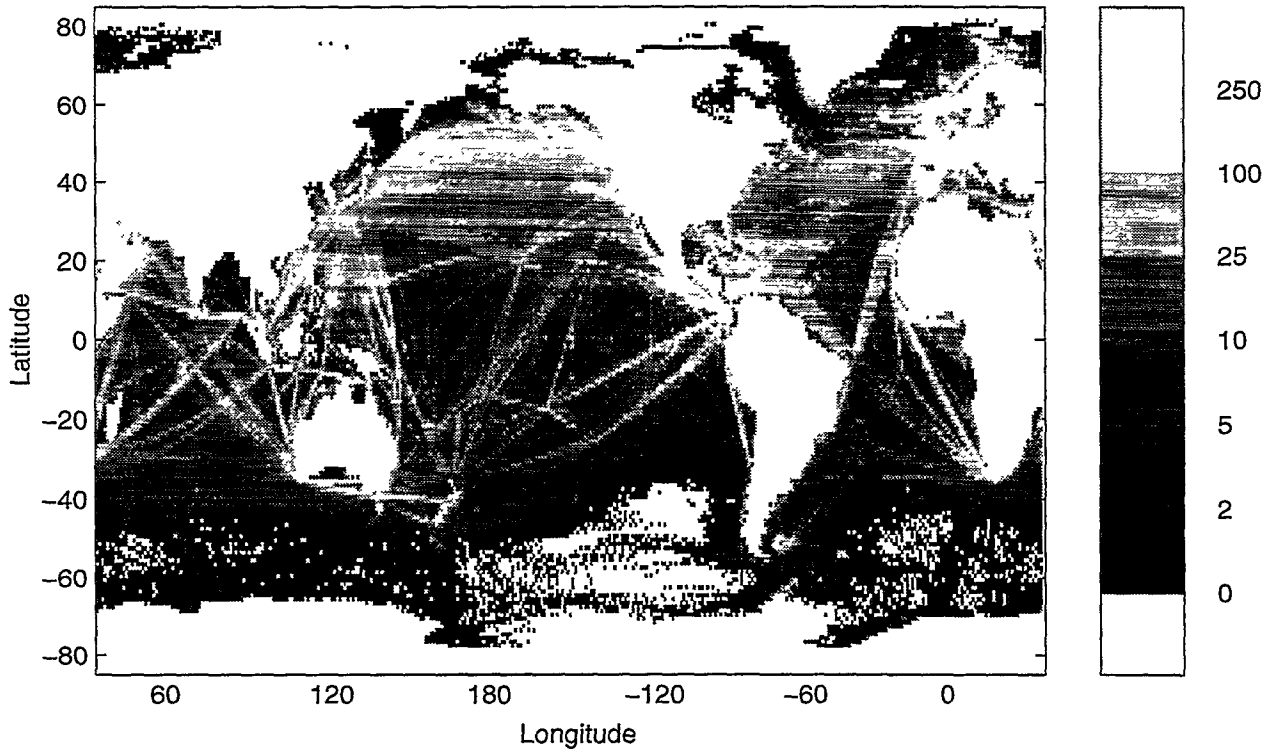

Figure 2) Global distribution of the number of latent heat flux estimates per 1^{o} x 1^{o} square used to form the average climatological monthly mean for the period 1980–1993. White indicates that there were no observations over the entire period considered.

Fig. 3a) Latent Heat Flux (W/m2), January

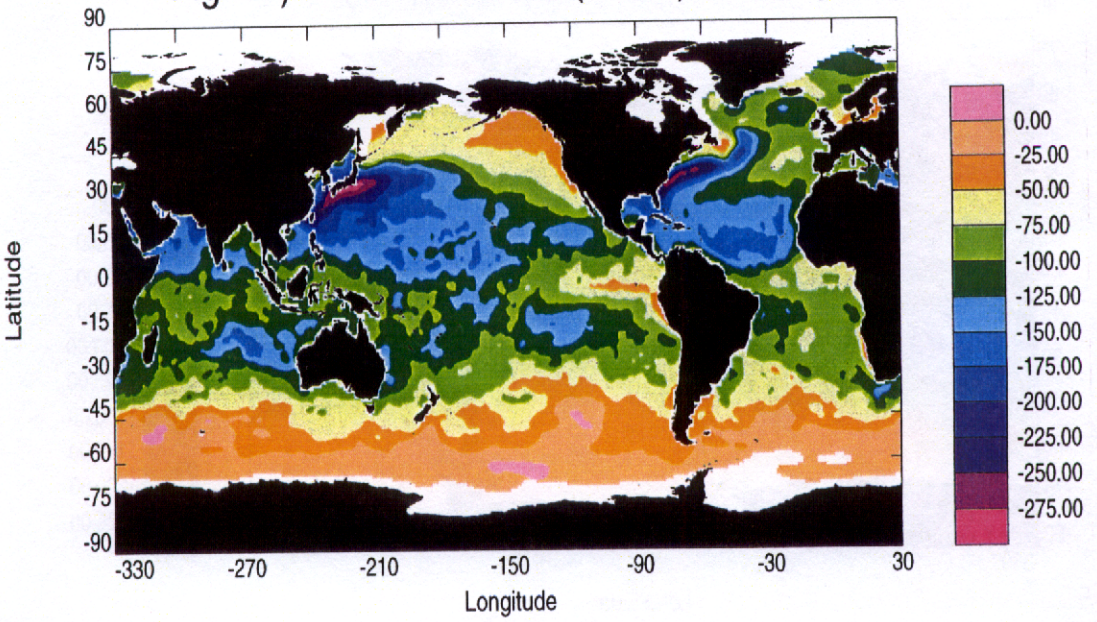

Fig. 3b) Latent Heat Flux (W/m2), April

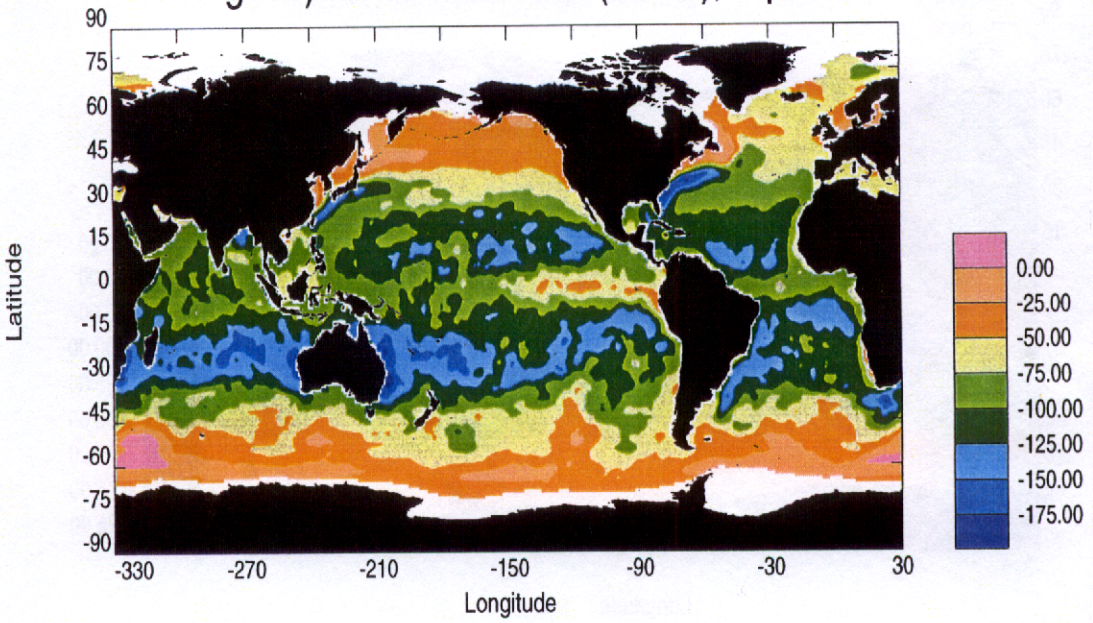

Fig. 3c) Latent Heat Flux (W/m2), July

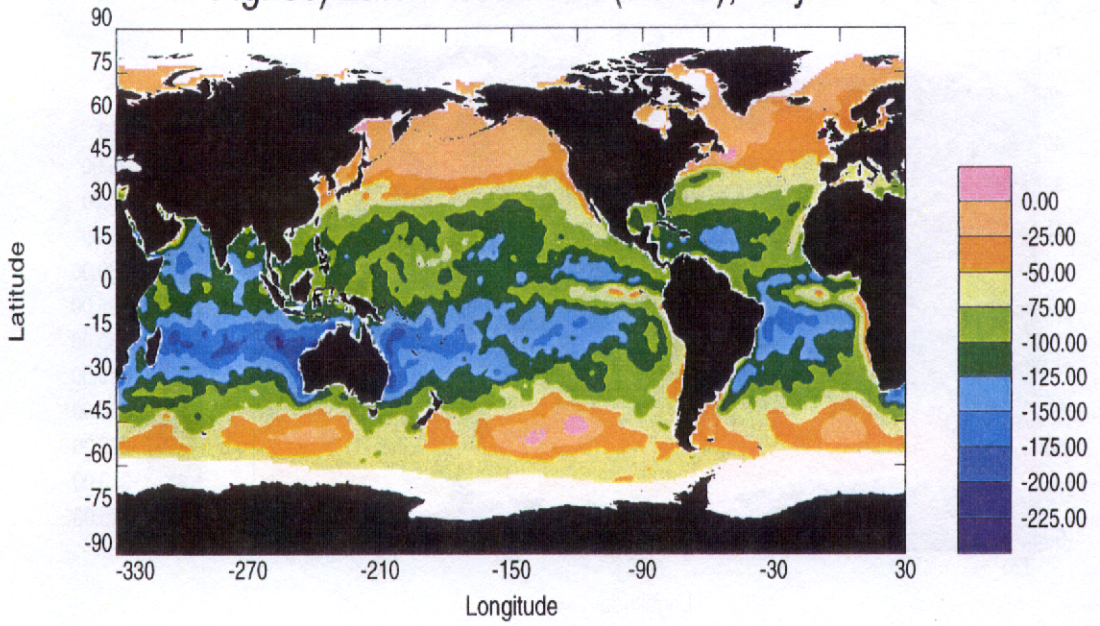

Fig. 3d) Latent Heat Flux (W/m2), October

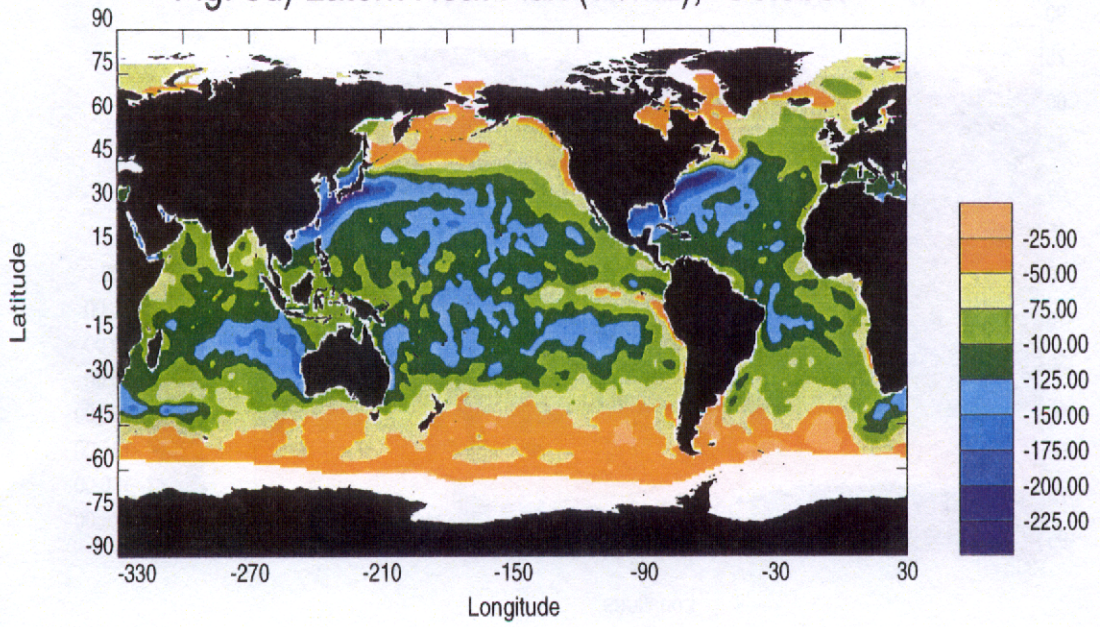

Fig. 4a) Sensible Heat Flux (W/m2), January

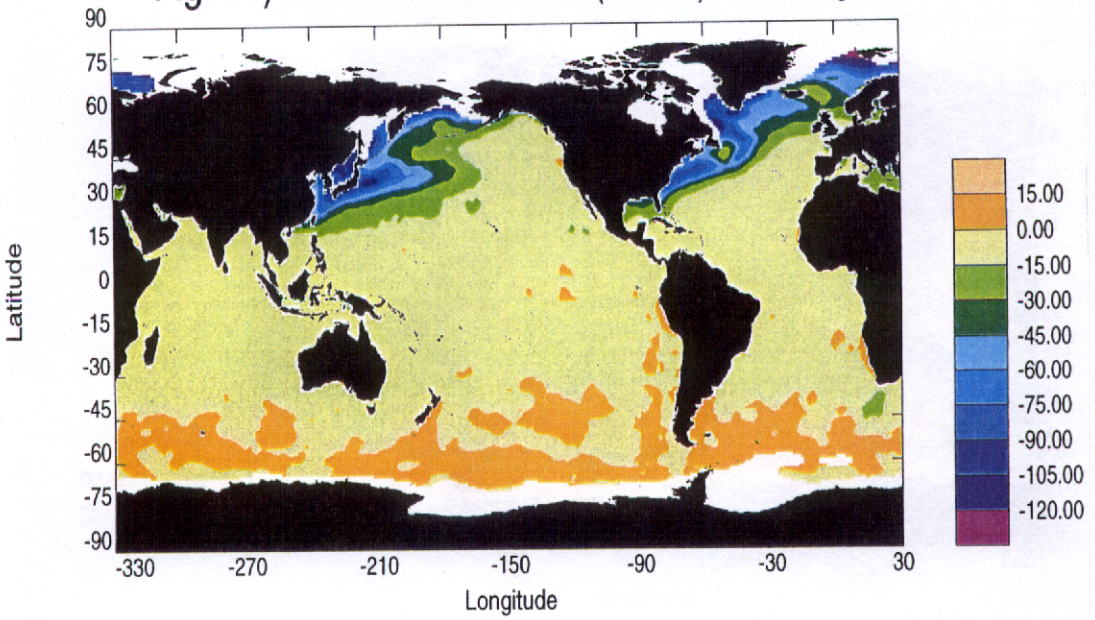

Fig. 4b) Sensible Heat Flux (W/m2), April

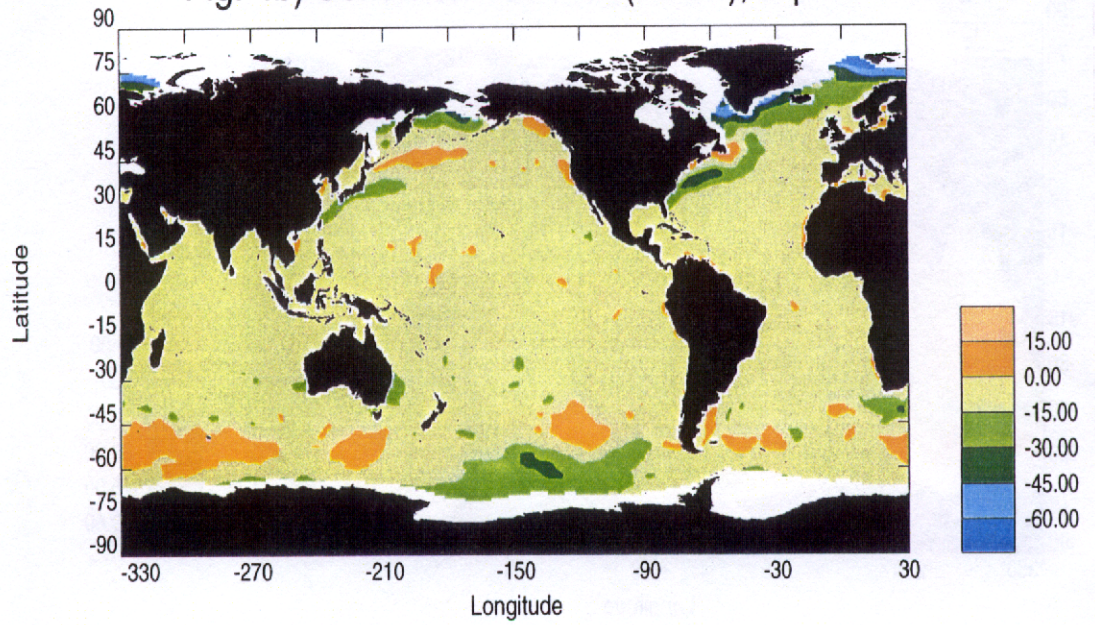

Fig. 4c) Sensible Heat Flux (W/m2), July

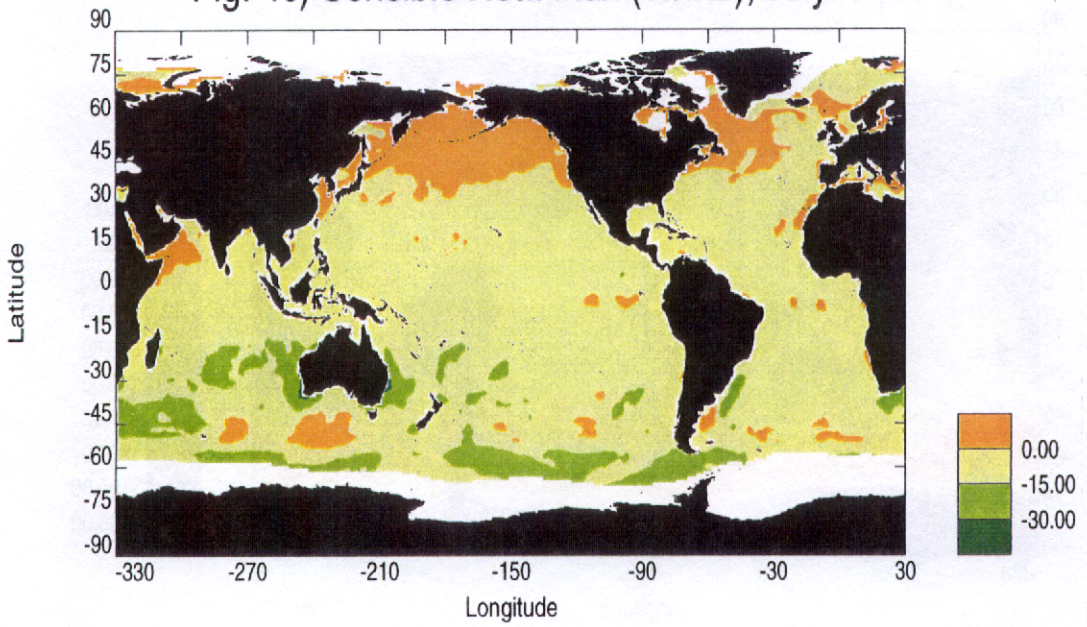

Fig. 4d) Sensible Heat Flux (W/m2), October

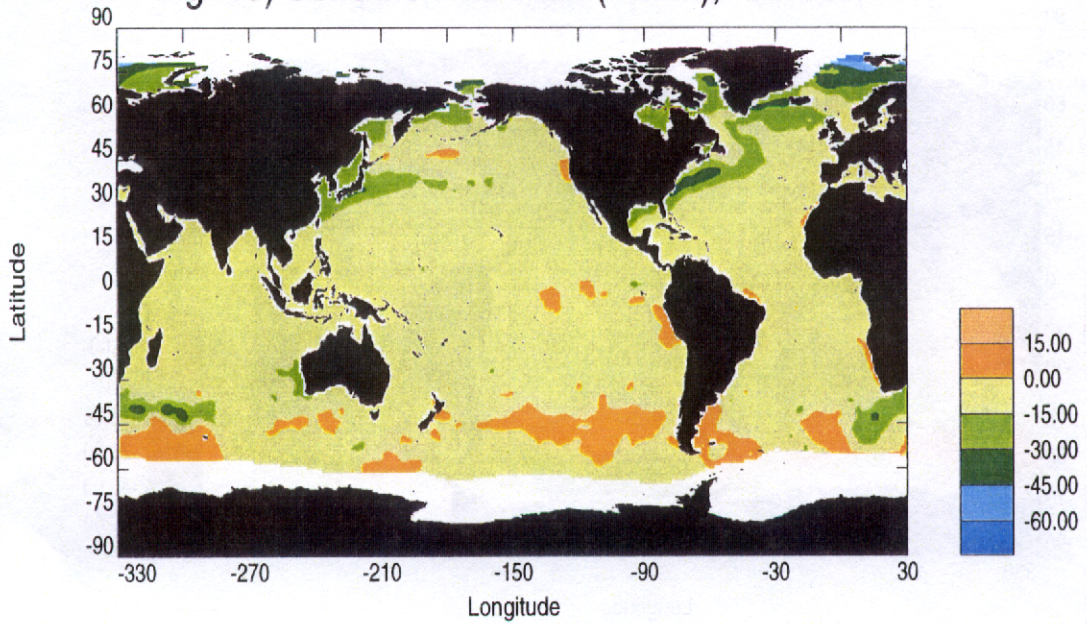

Fig. 5a) Longwave Flux (W/m2), January

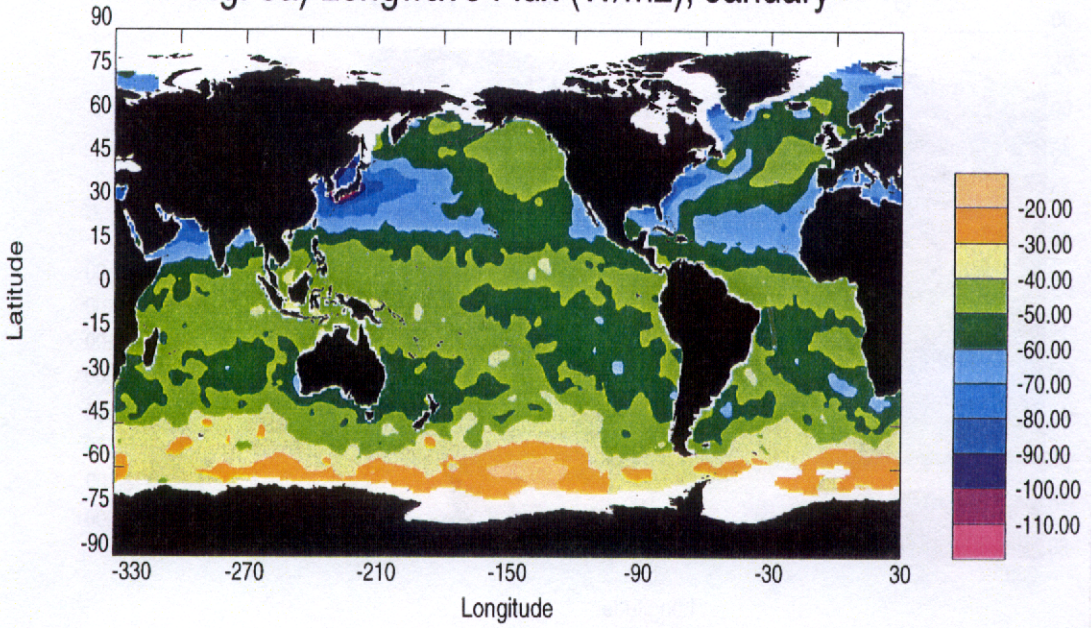

Fig. 5b) Longwave Flux (W/m2), April

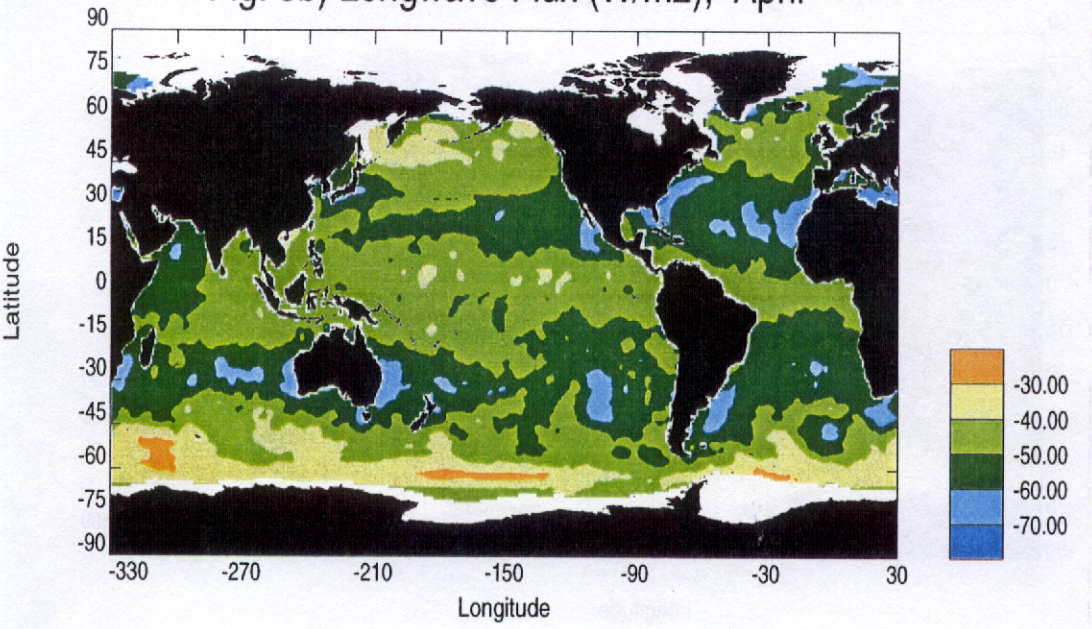

Fig. 5c) Longwave Flux (W/m2), July

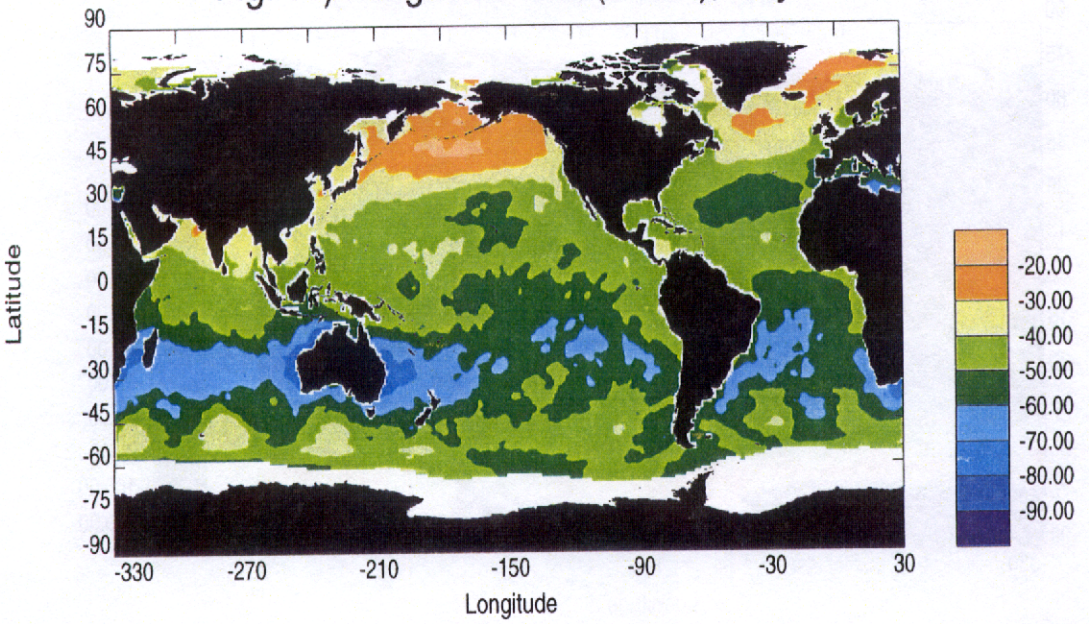

Fig. 5d) Longwave Flux (W/m2), October

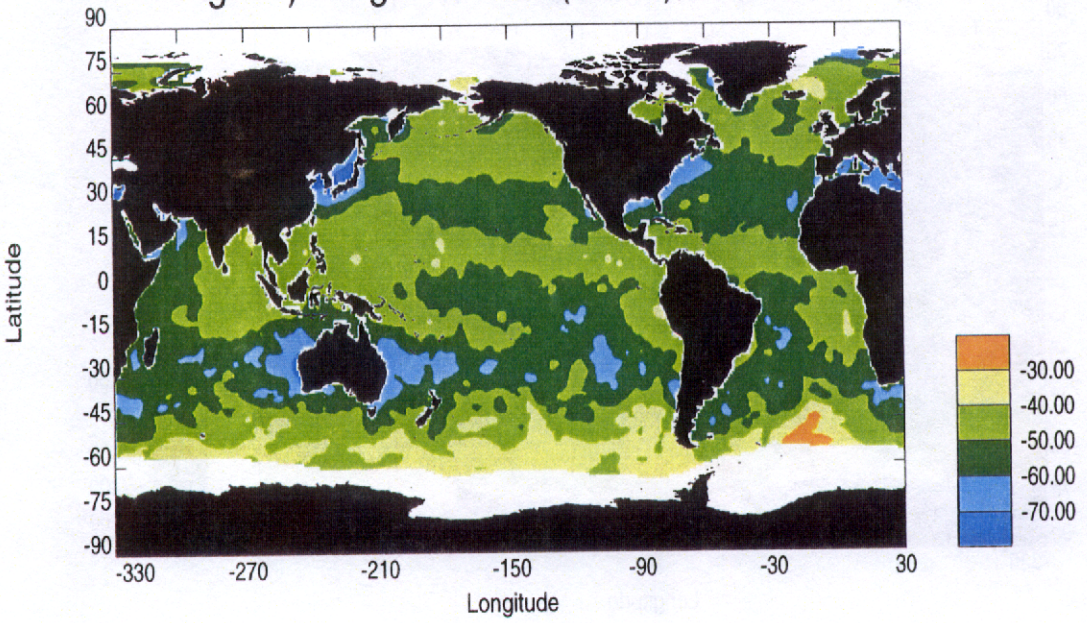

Fig. 6a) Shortwave Flux (W/m2), January

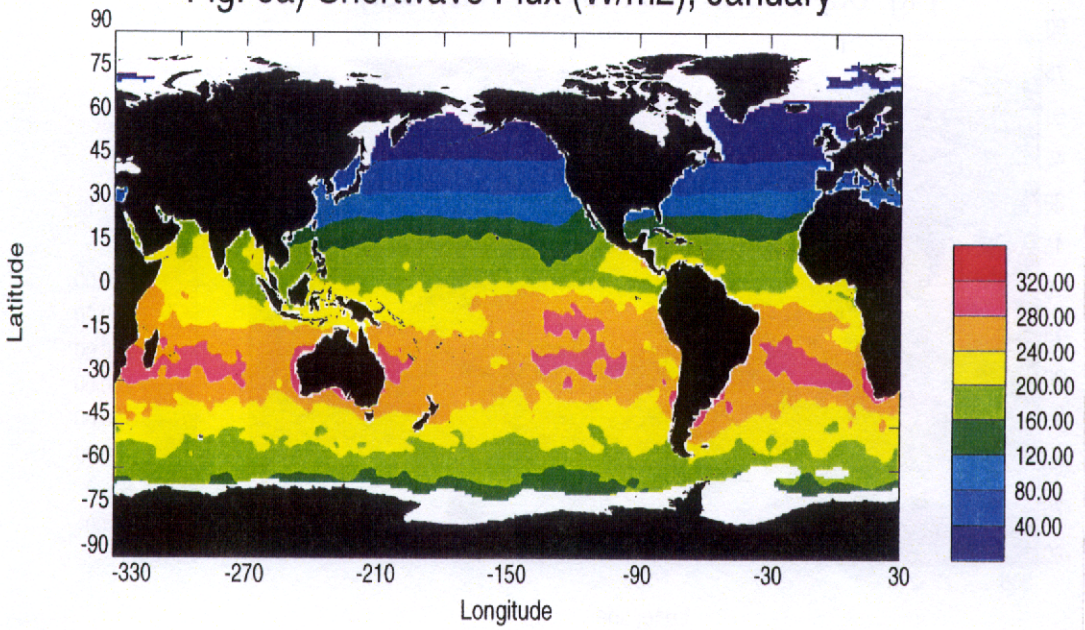

Fig. 6b) Shortwave Flux (W/m2), April

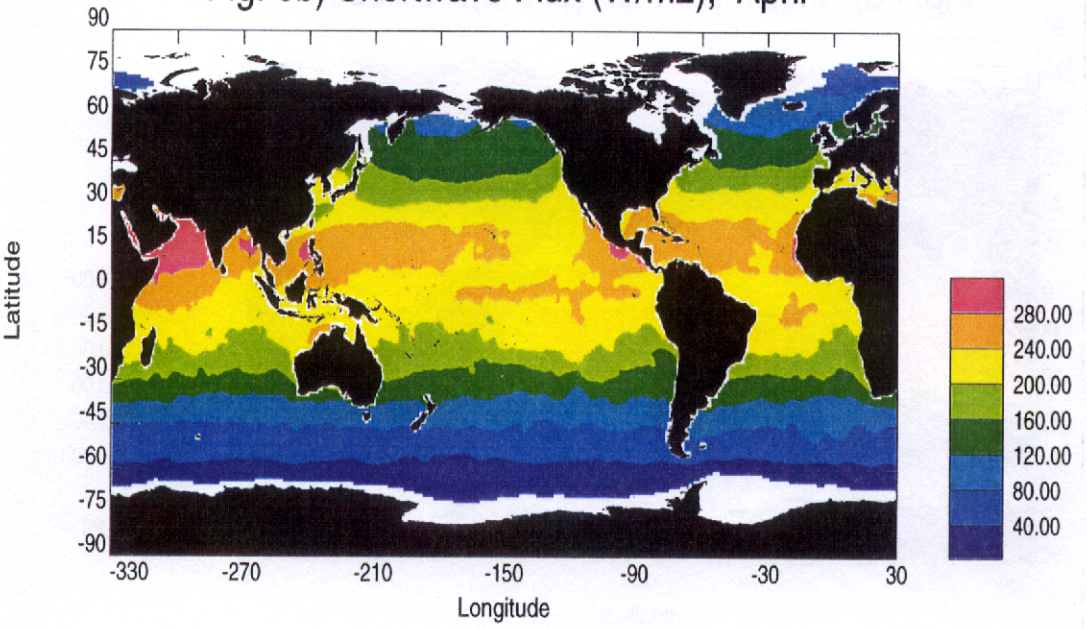

Fig. 6c) Shortwave Flux (W/m2), July

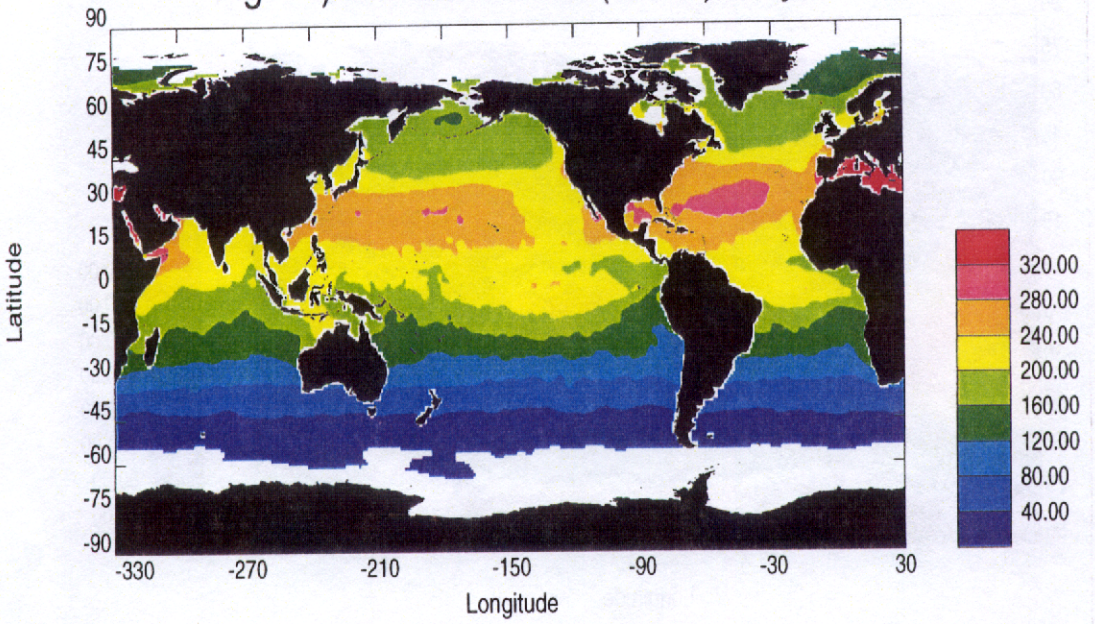

Fig. 6d) Shortwave Flux (W/m2), October

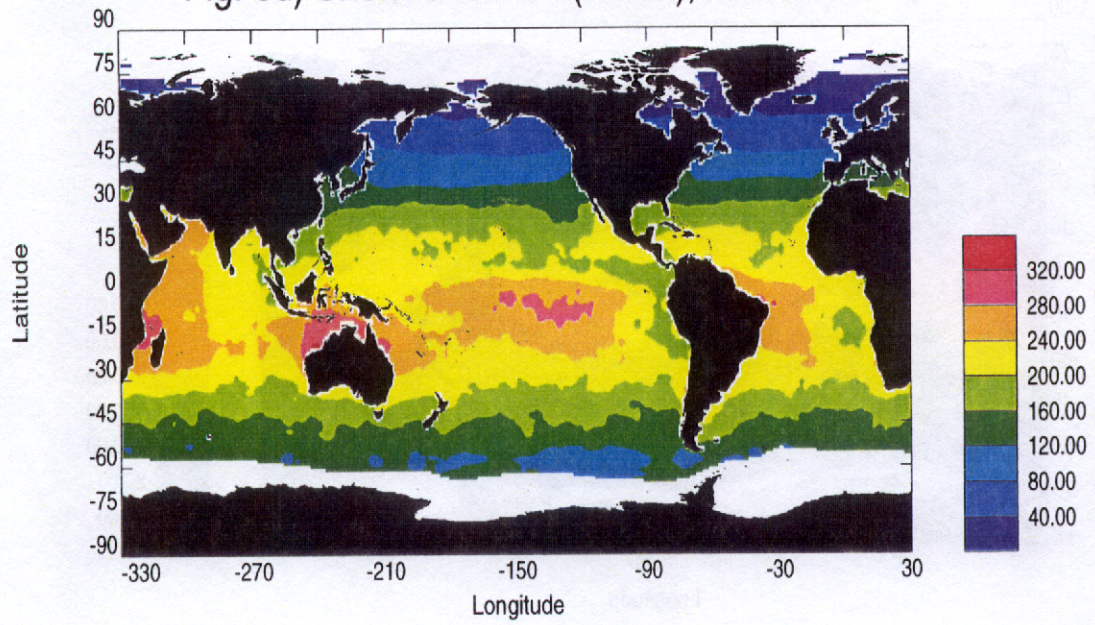

Fig. 7a) Net Heat Flux (W/m2), January

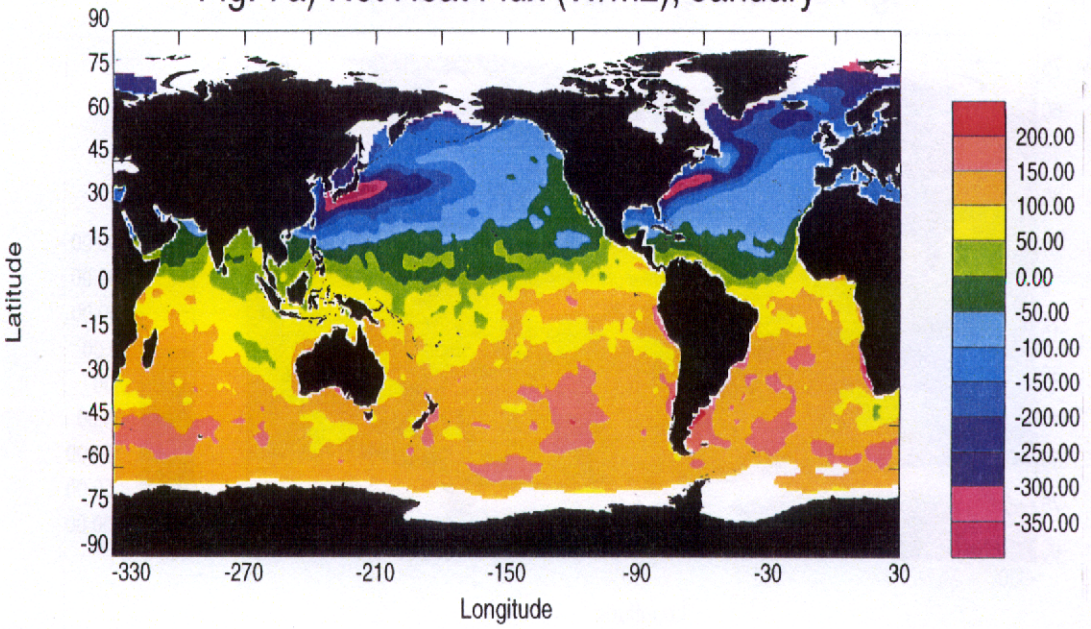

Fig. 7b) Net Heat Flux (W/m2), April

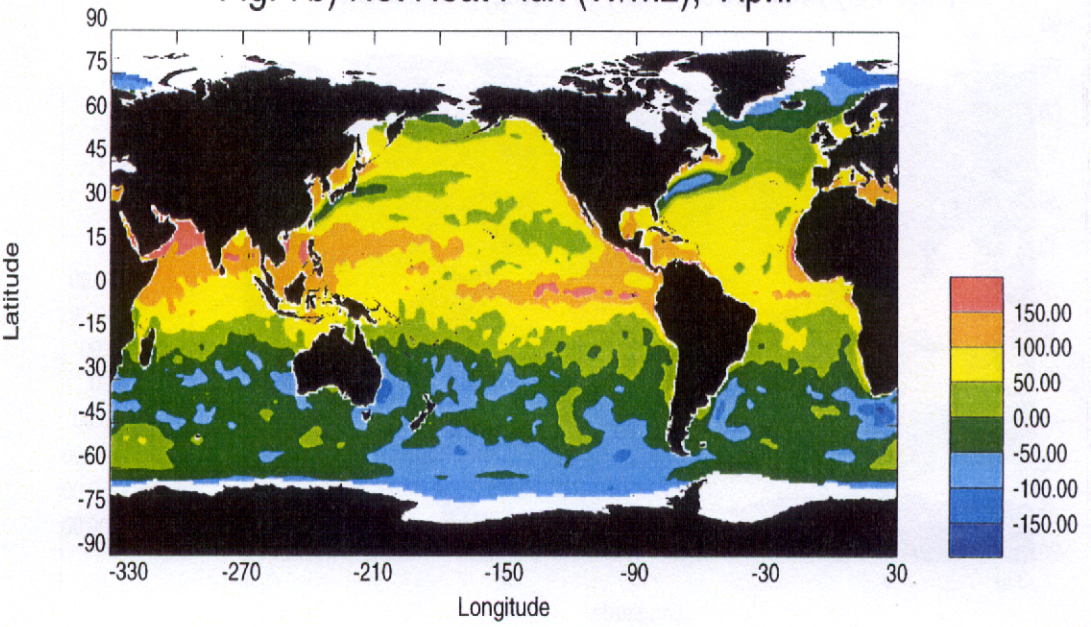

Fig. 7c) Net Heat Flux (W/m2), July

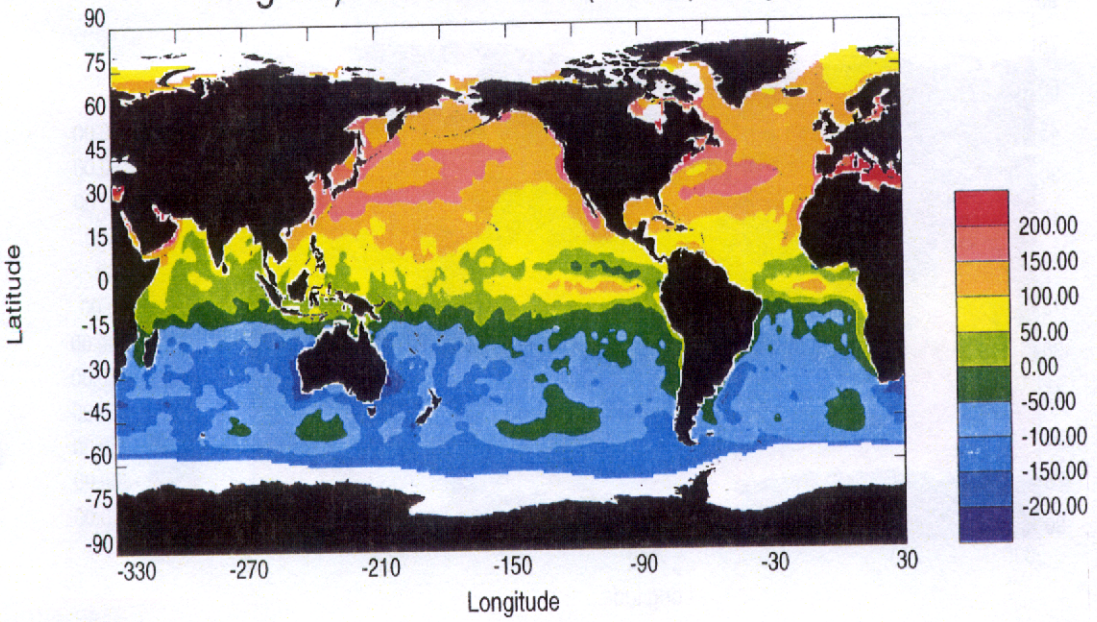

Fig. 7d) Net Heat Flux (W/m2), October

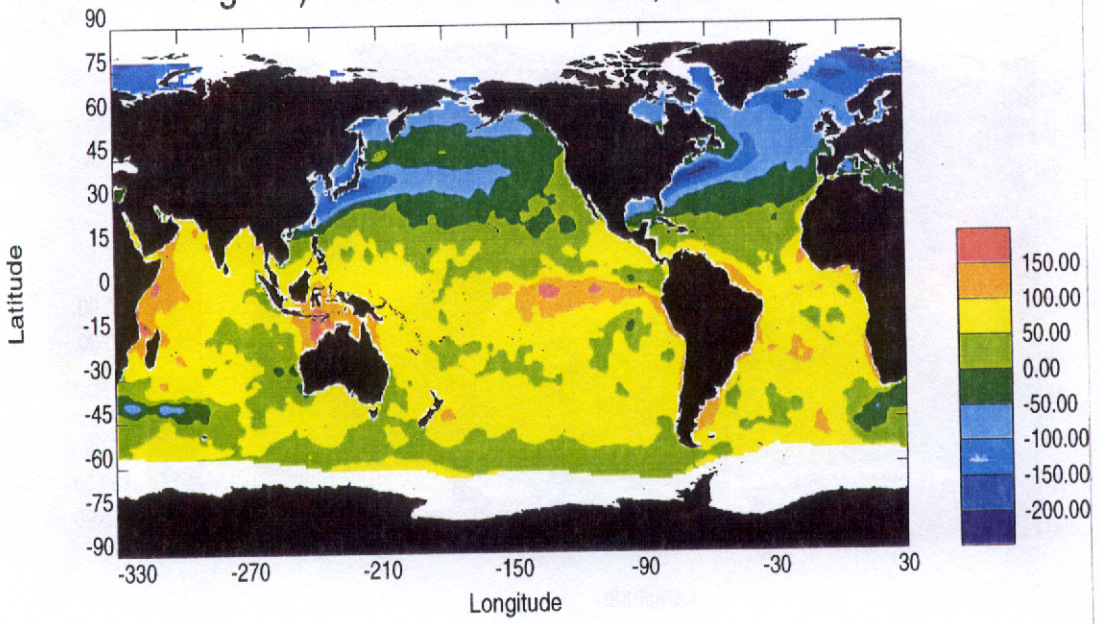

Fig. 8a) Wind Stress (N/m2), January

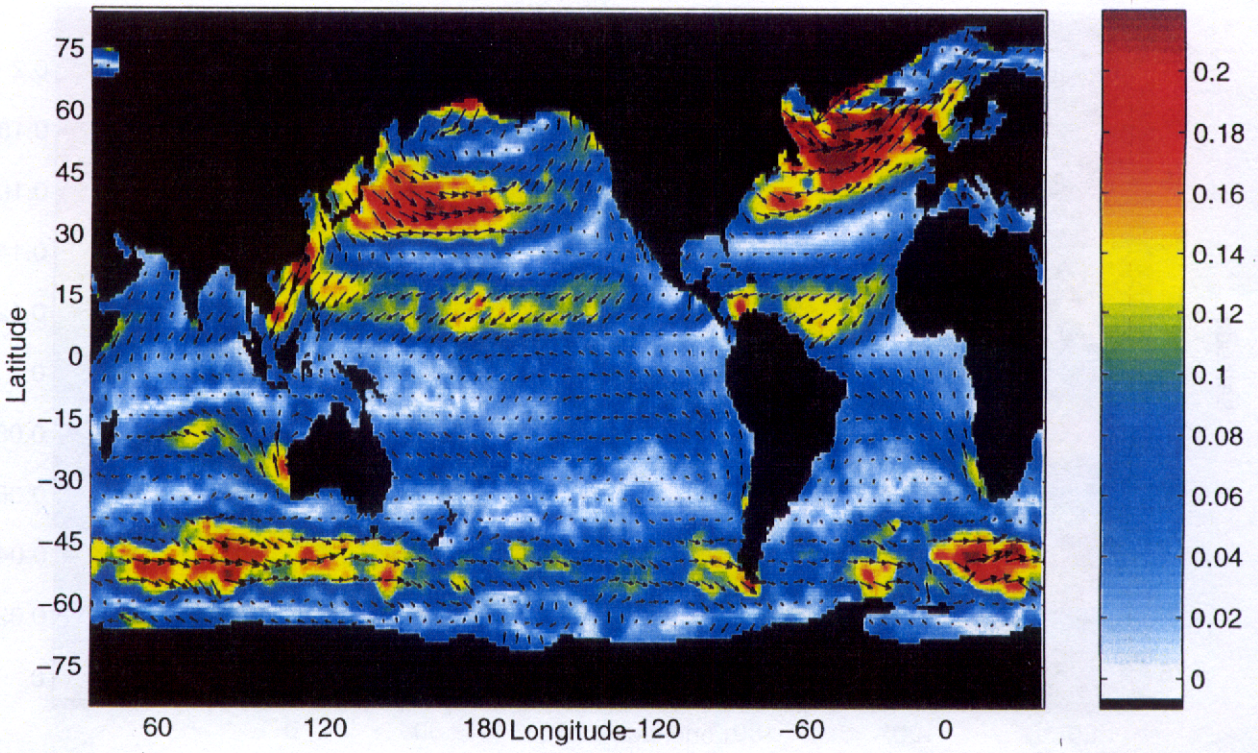

Fig. 8b) Wind Stress (N/m2), April

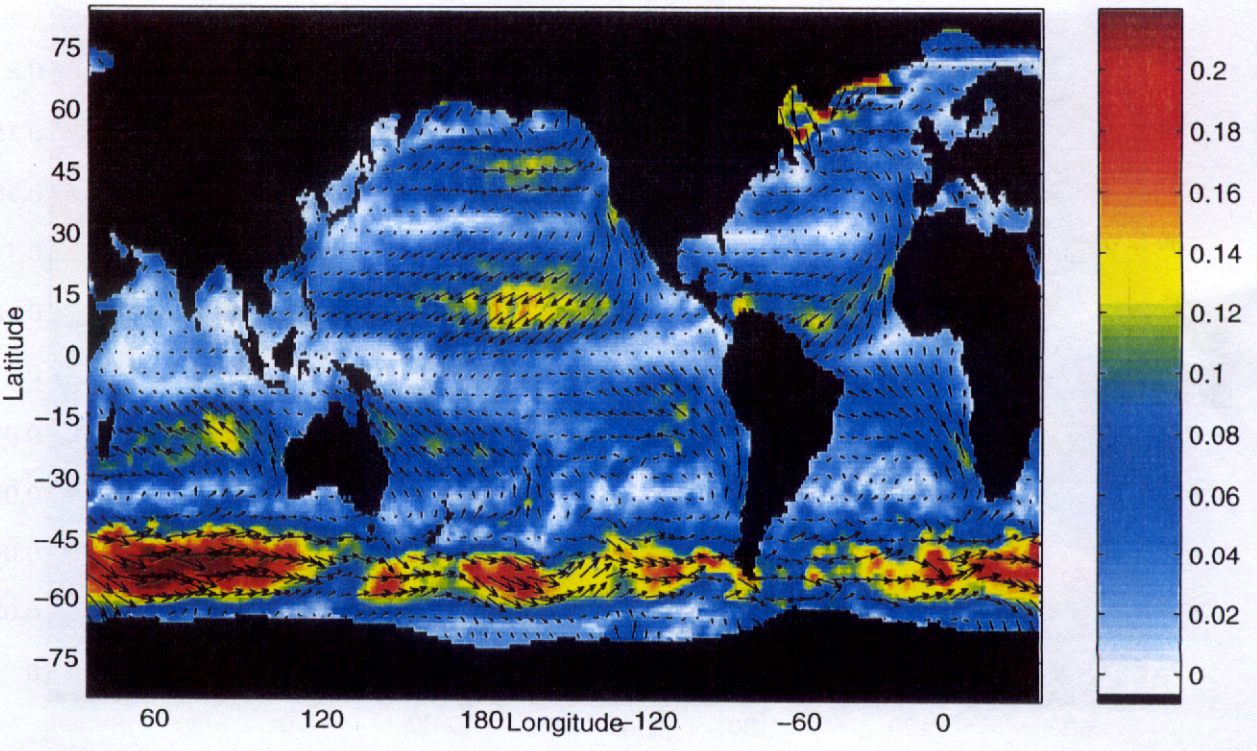

Fig. 8c) Wind Stress (N/m2), July

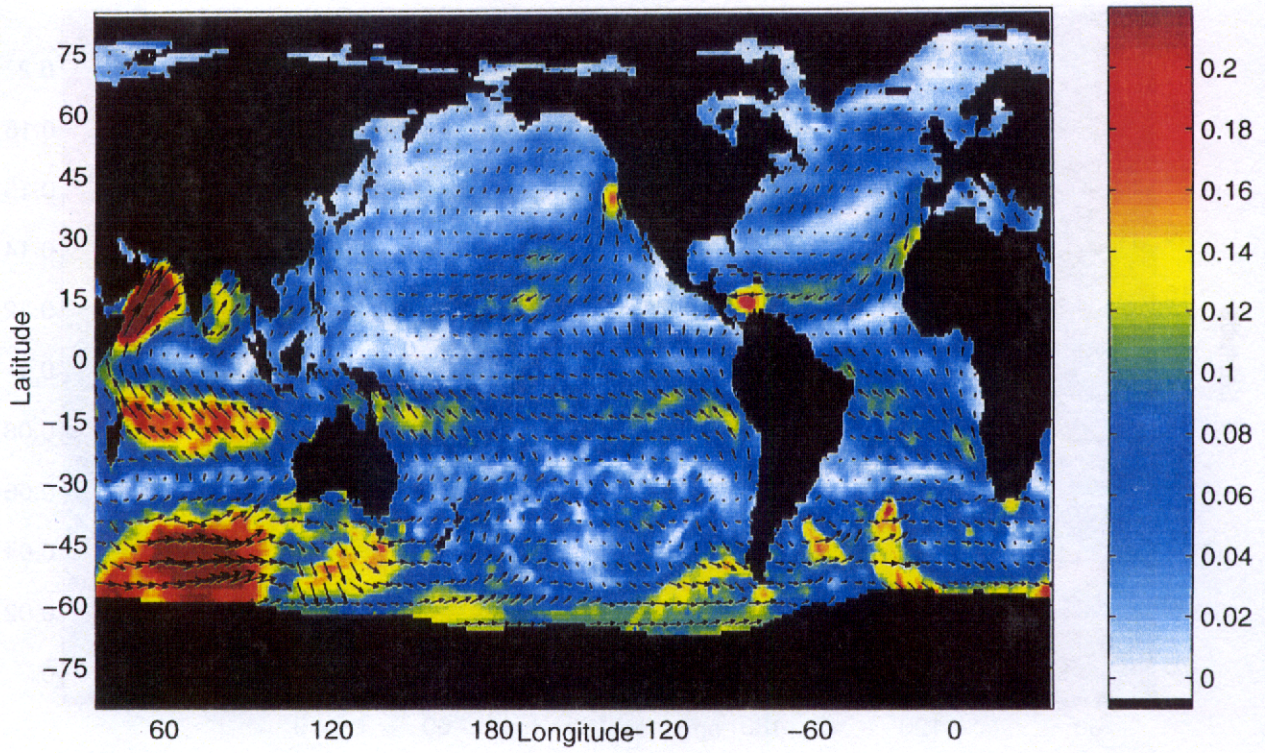

Fig. 8d) Wind Stress (N/m2), October

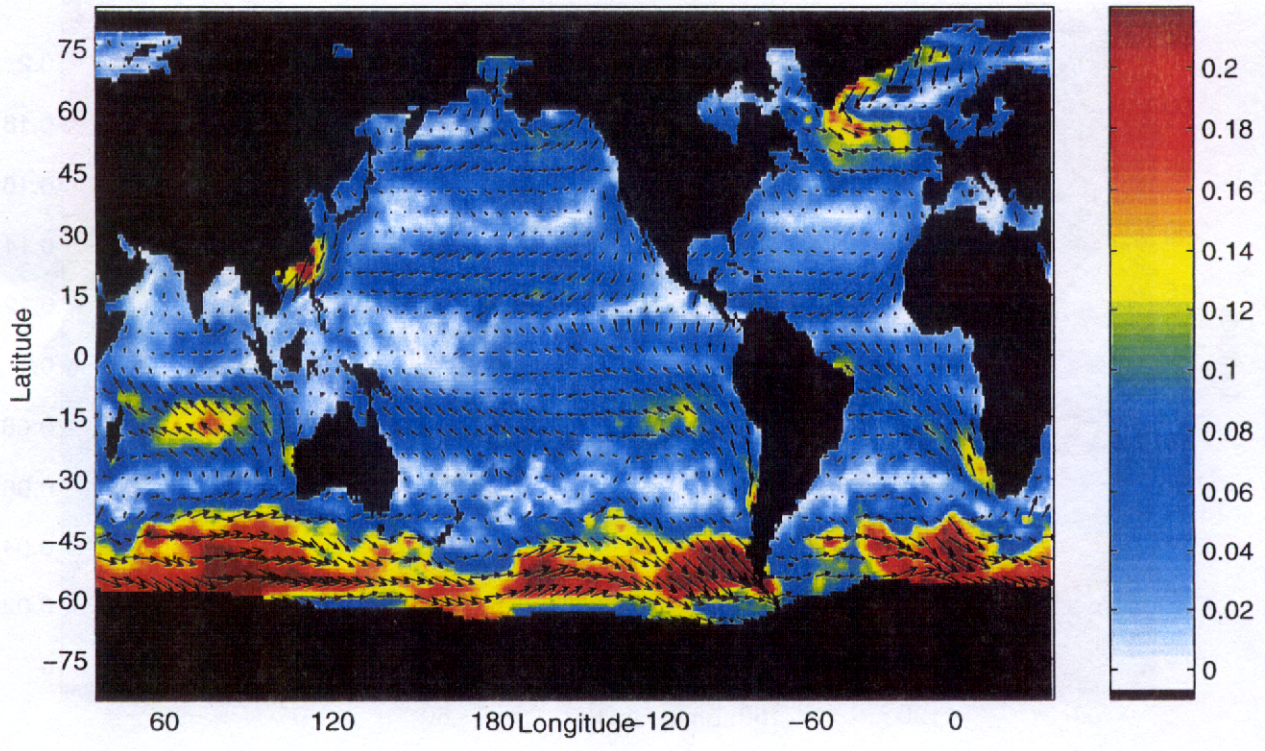

Fig. 9a) Precipitation (mm/month), January

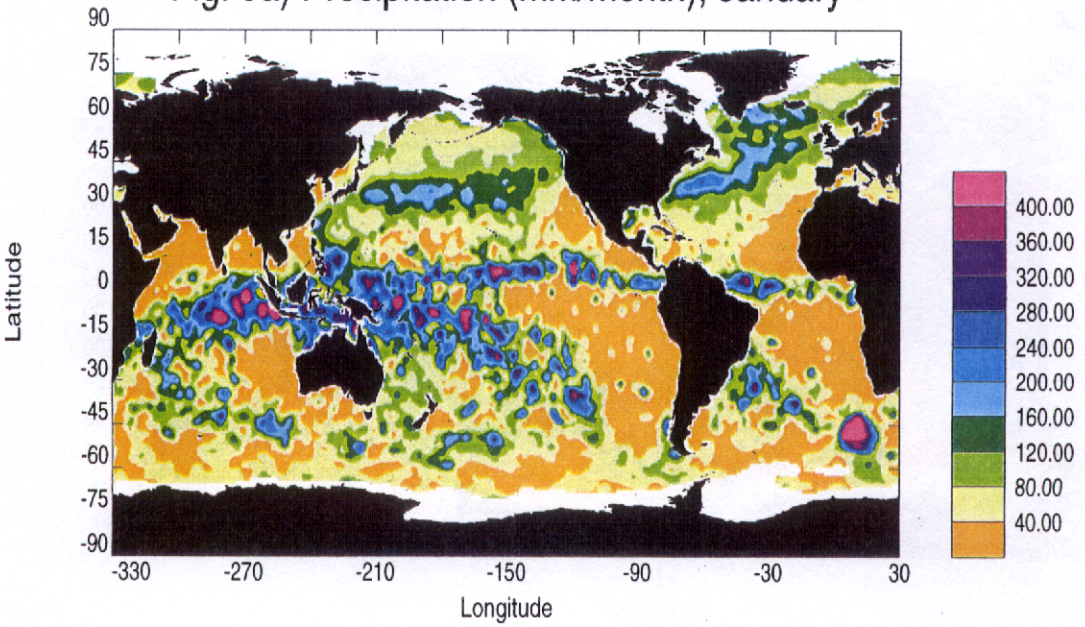

Fig. 9b) Precipitation (mm/month), April

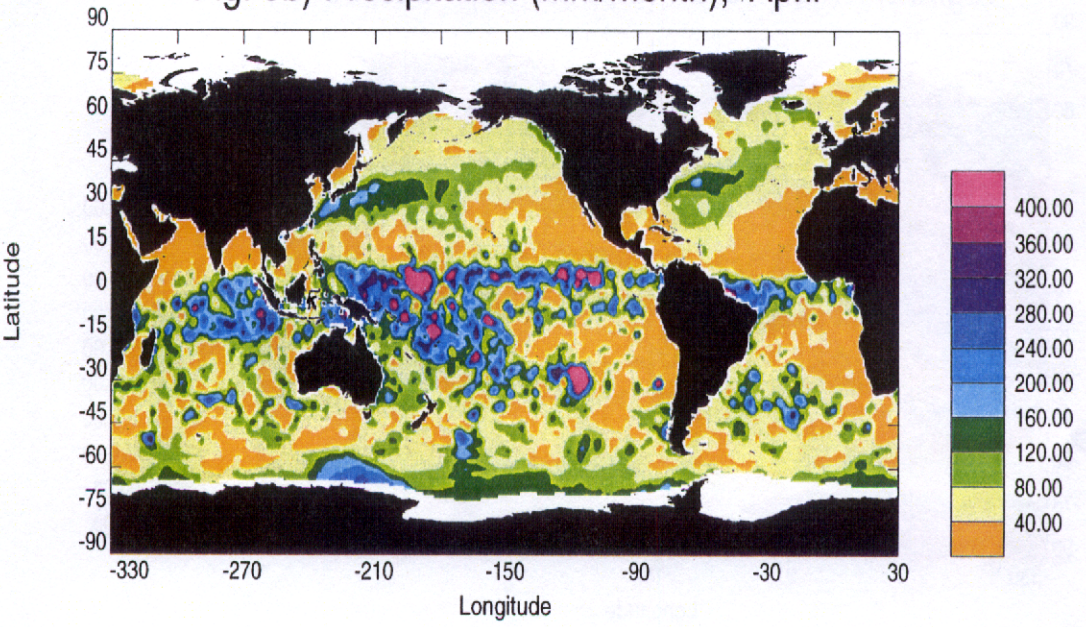

Fig. 9c) Precipitation (mm/month), July

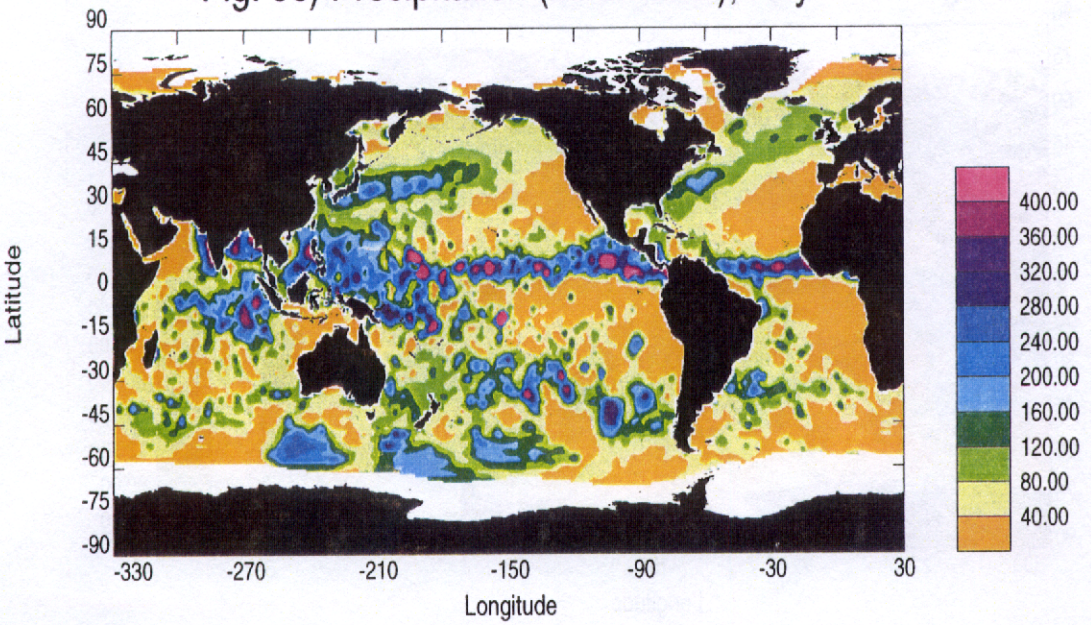

Fig. 9d) Precipitation (mm/month), October

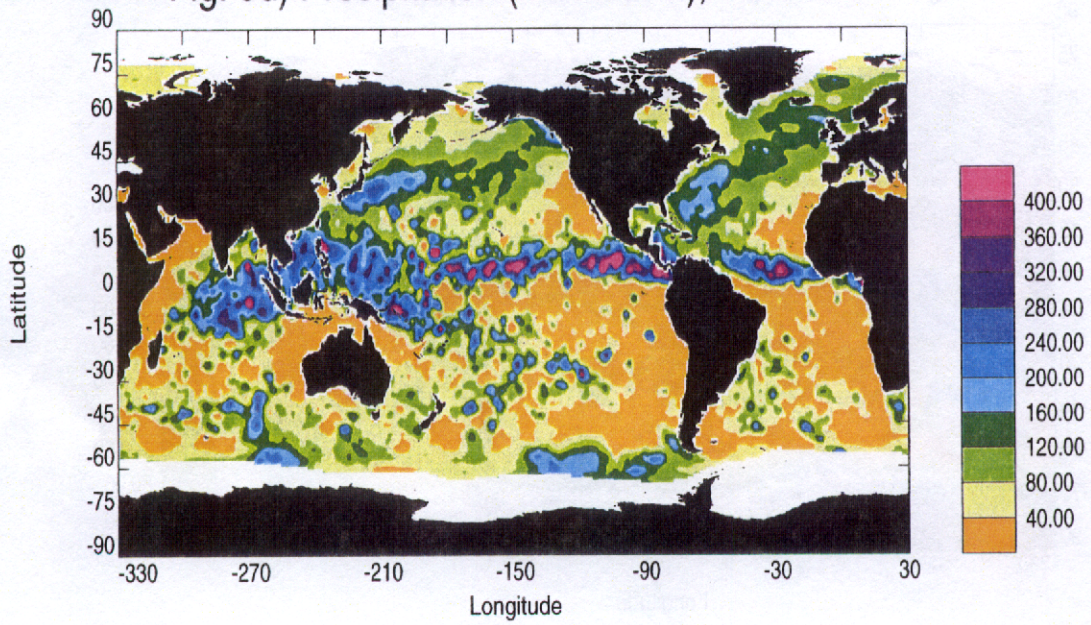

Fig. 10a) Net Evaporation (mm/month), January

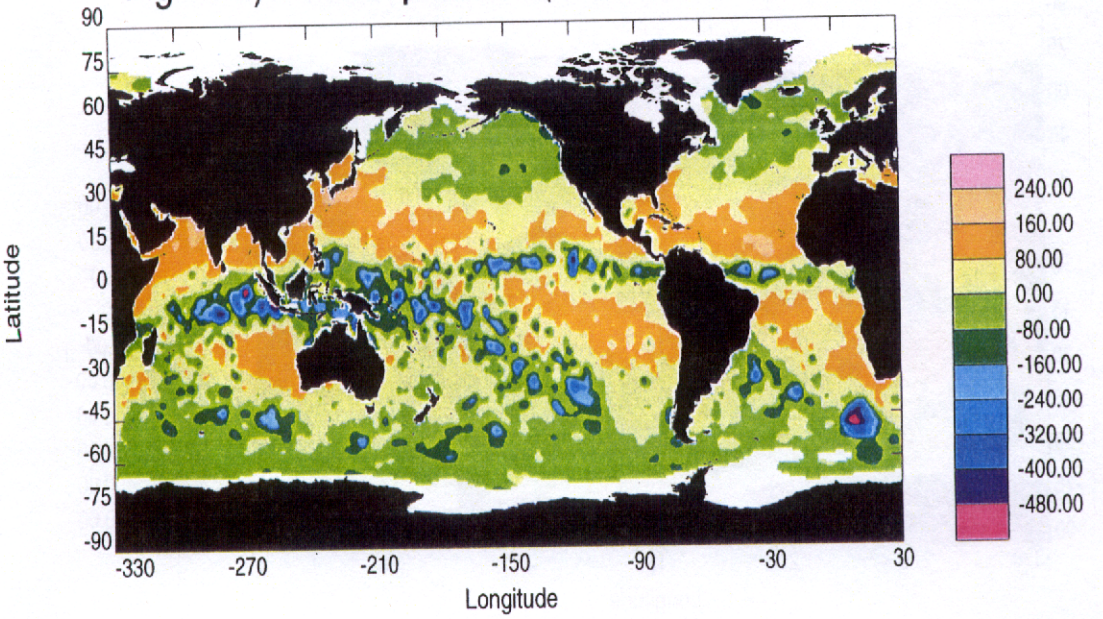

Fig. 10b) Net Evaporation (mm/month), April

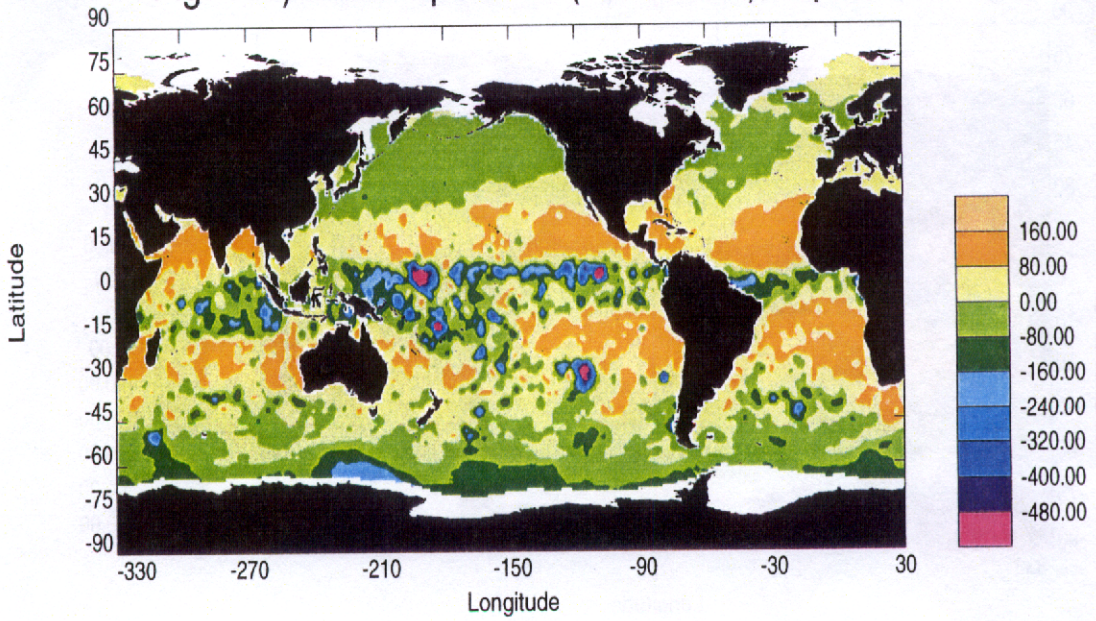

Fig. 10c) Net Evaporation (mm/month), July

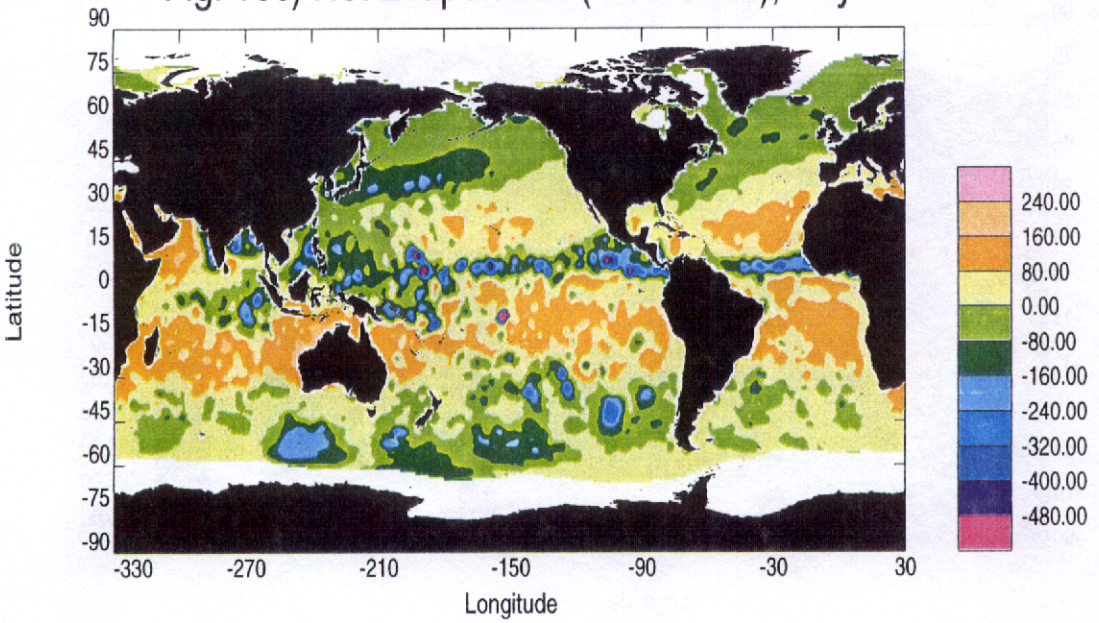

Fig. 10d) Net Evaporation (mm/month), October

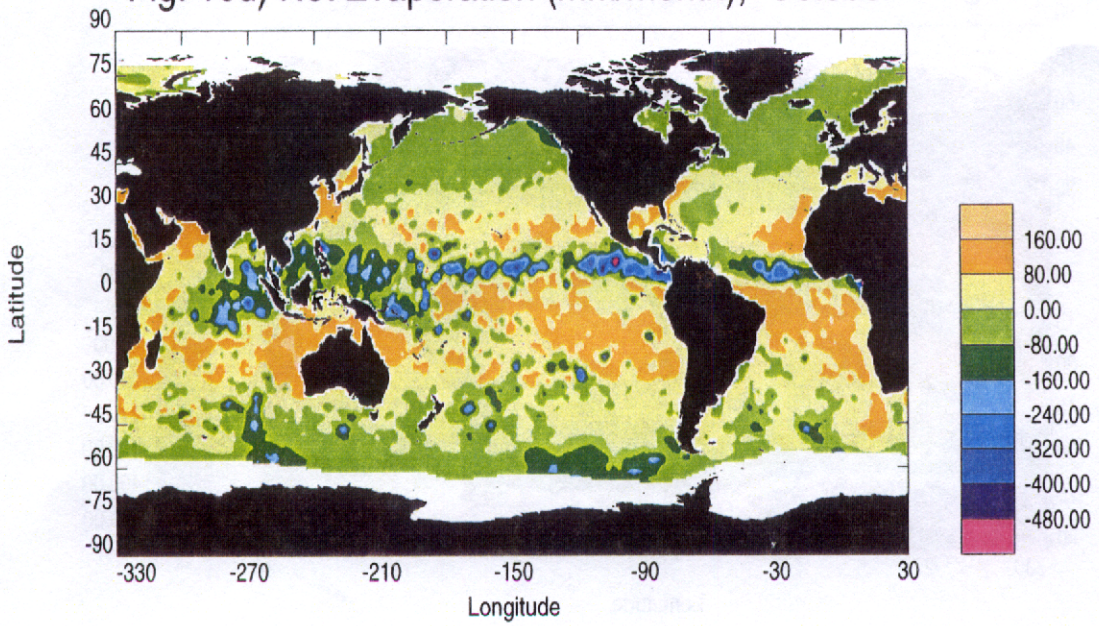

Fig. 11a)

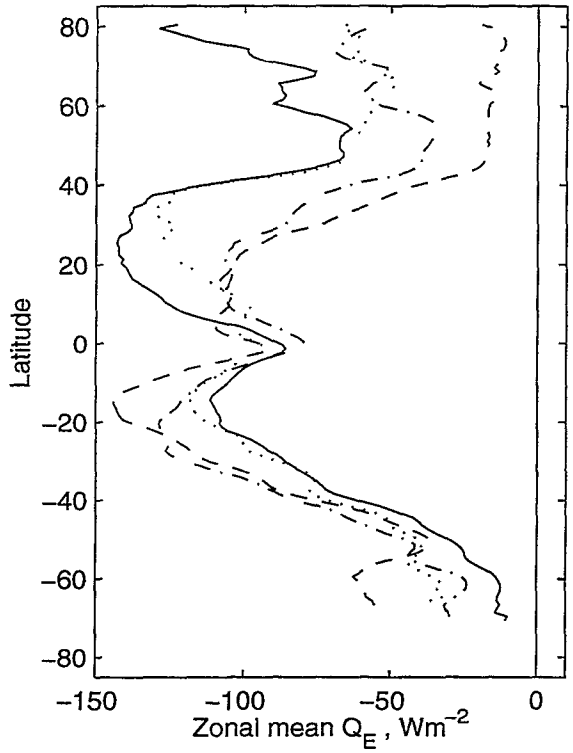

Fig. 11b)

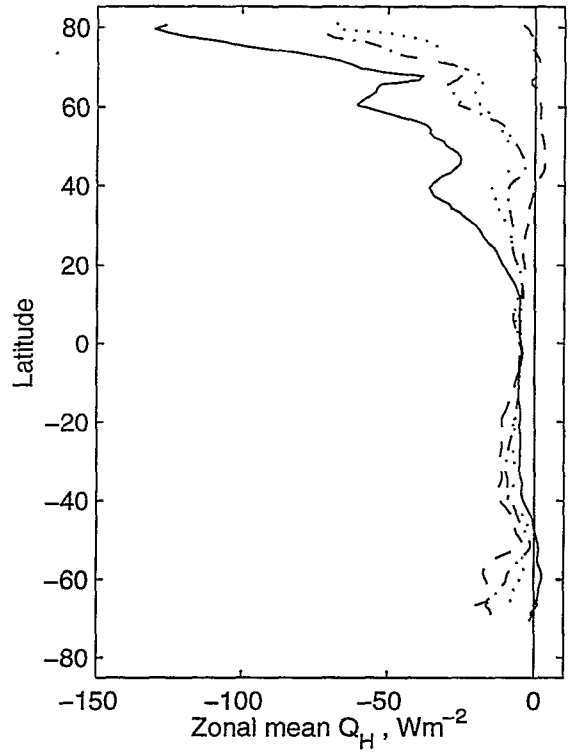

Fig. 11c)

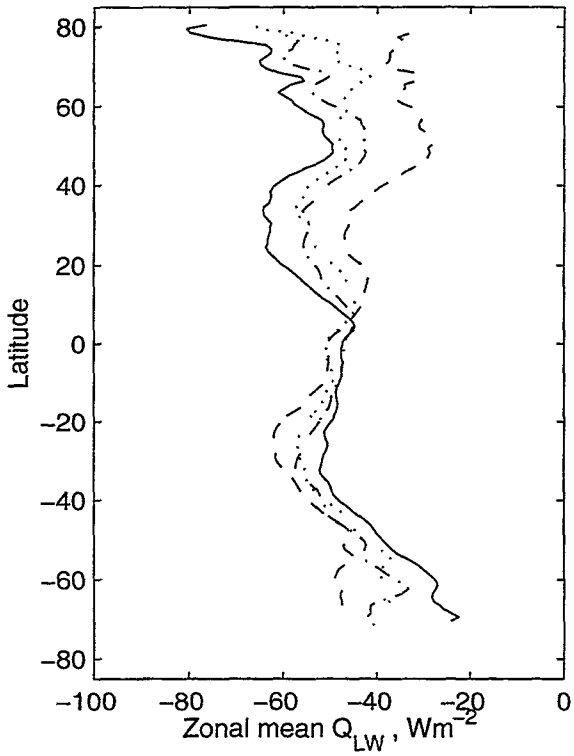

Fig. 11d)

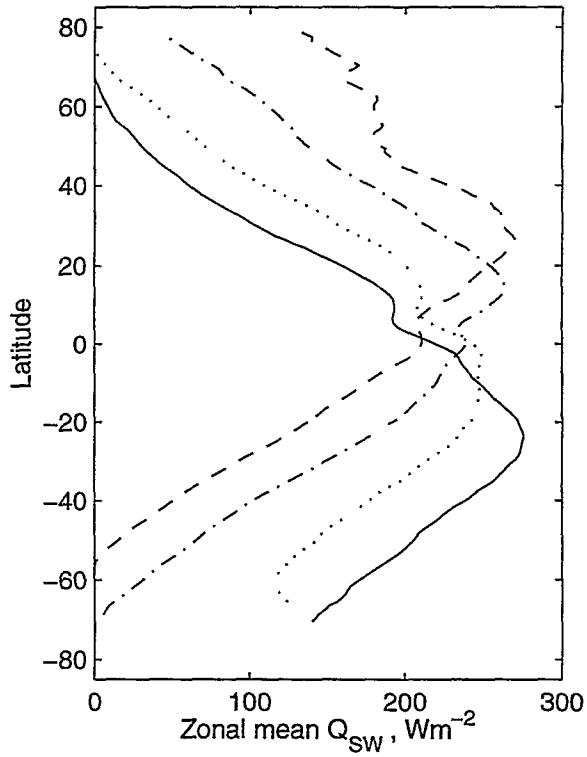

Fig. 11e)

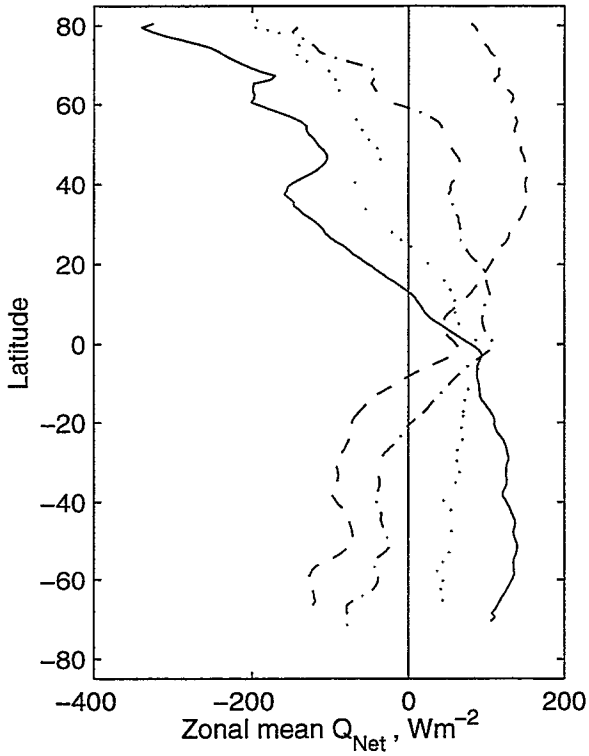

Fig. 11f)

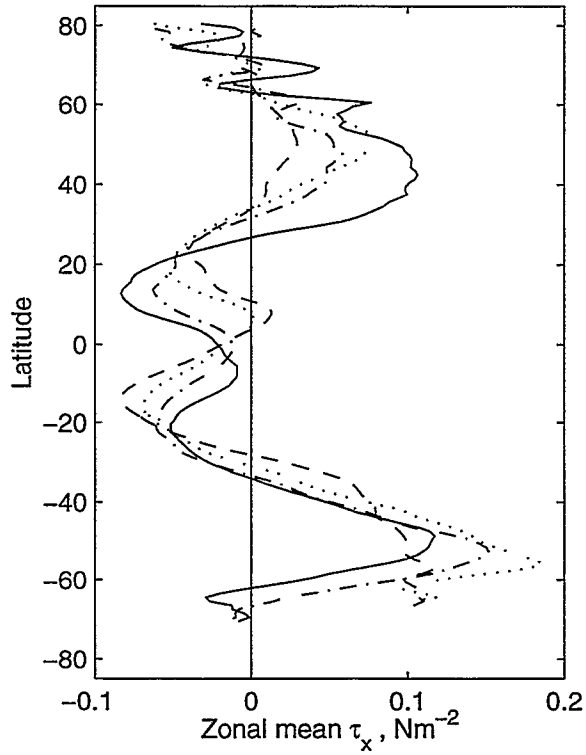

Fig. 11g)

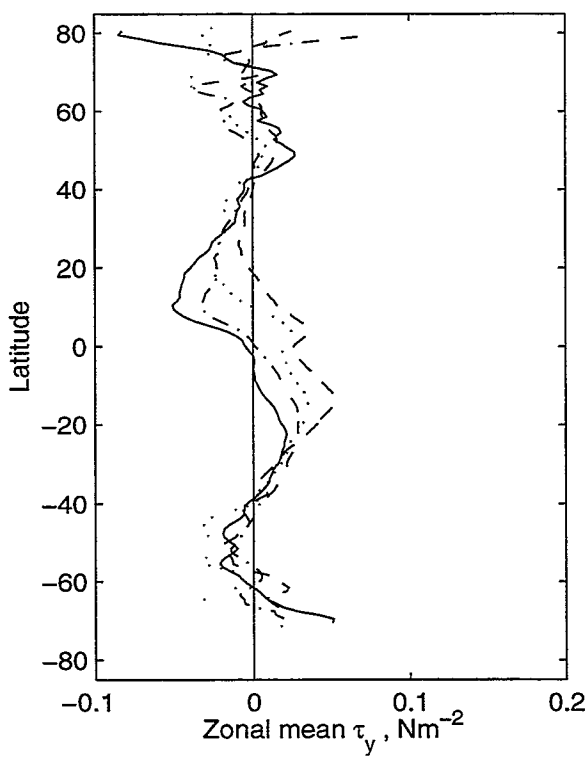

Fig. 11h)

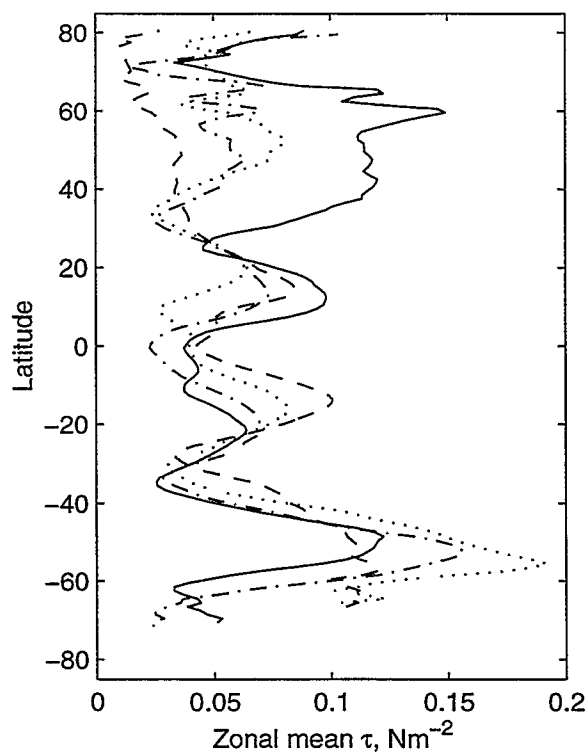

Fig. 11i)

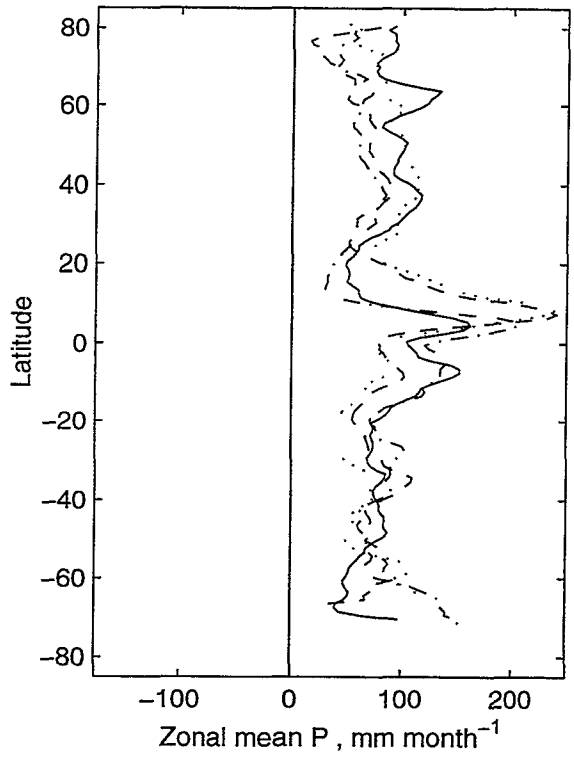

Fig. 11j)

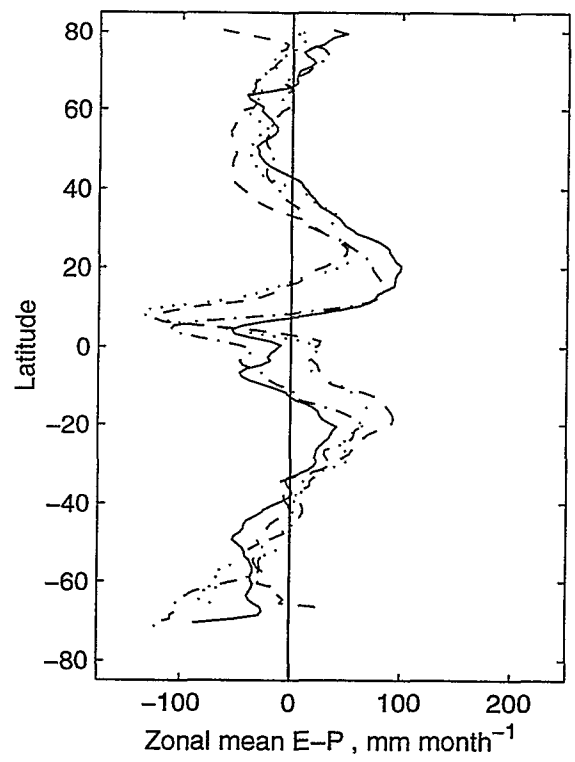

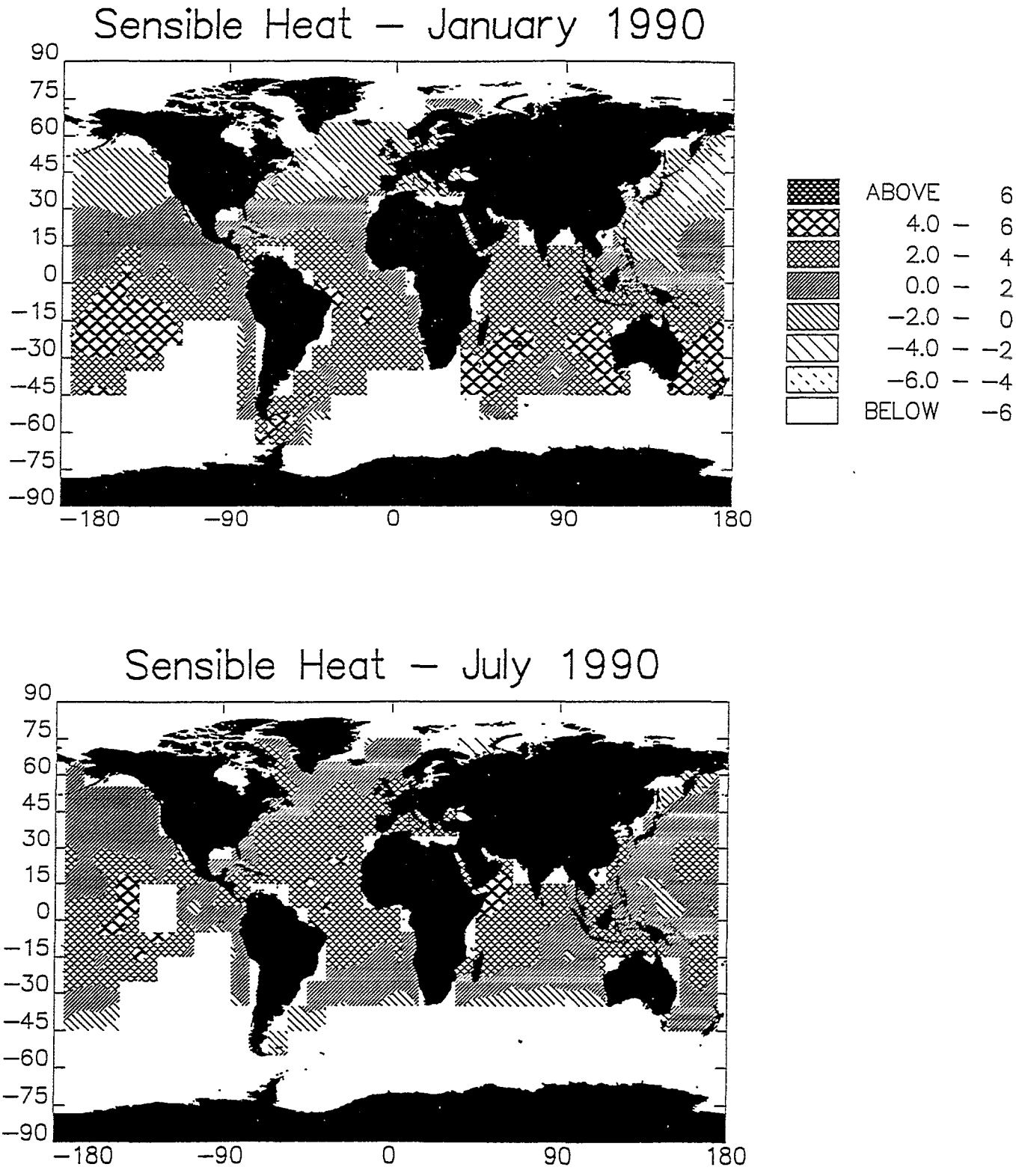

Figure 12a-b) Global distribution of the difference between the fully corrected and uncorrected sensible heat flux fields for January and July 1990. Units Wm^{-2}.

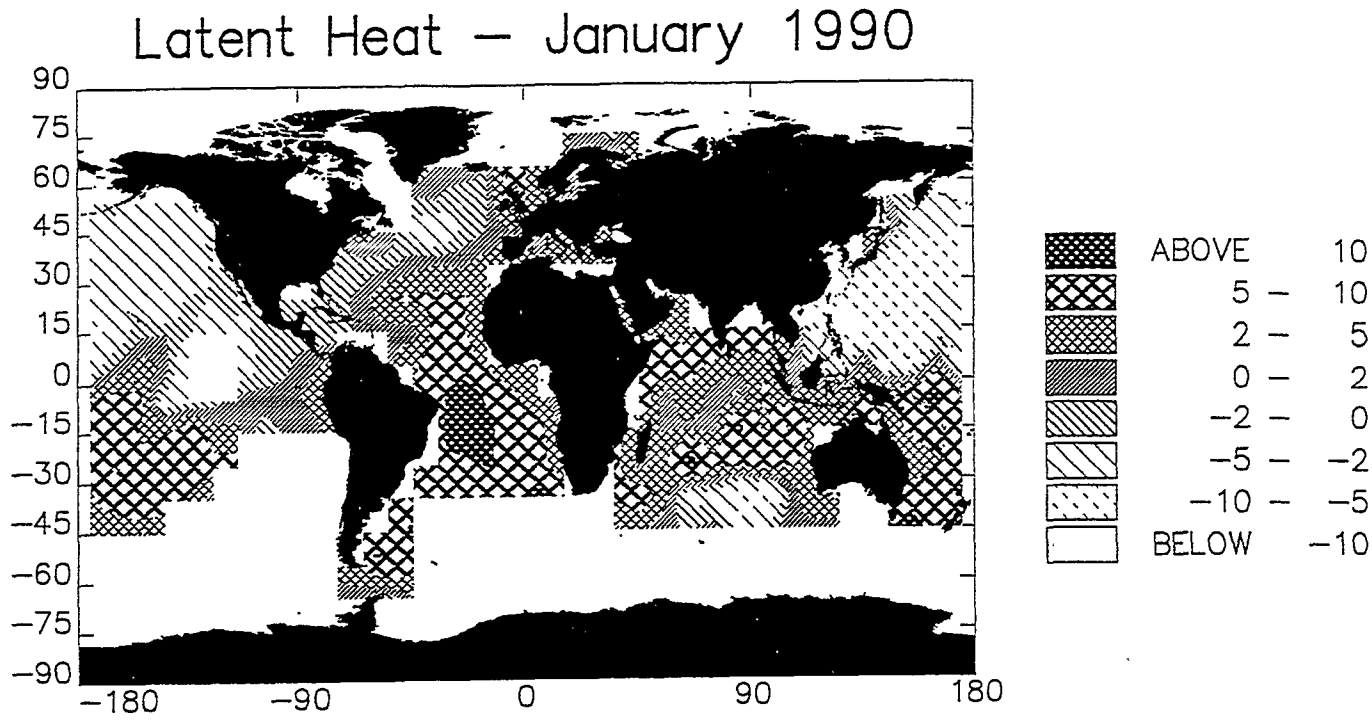

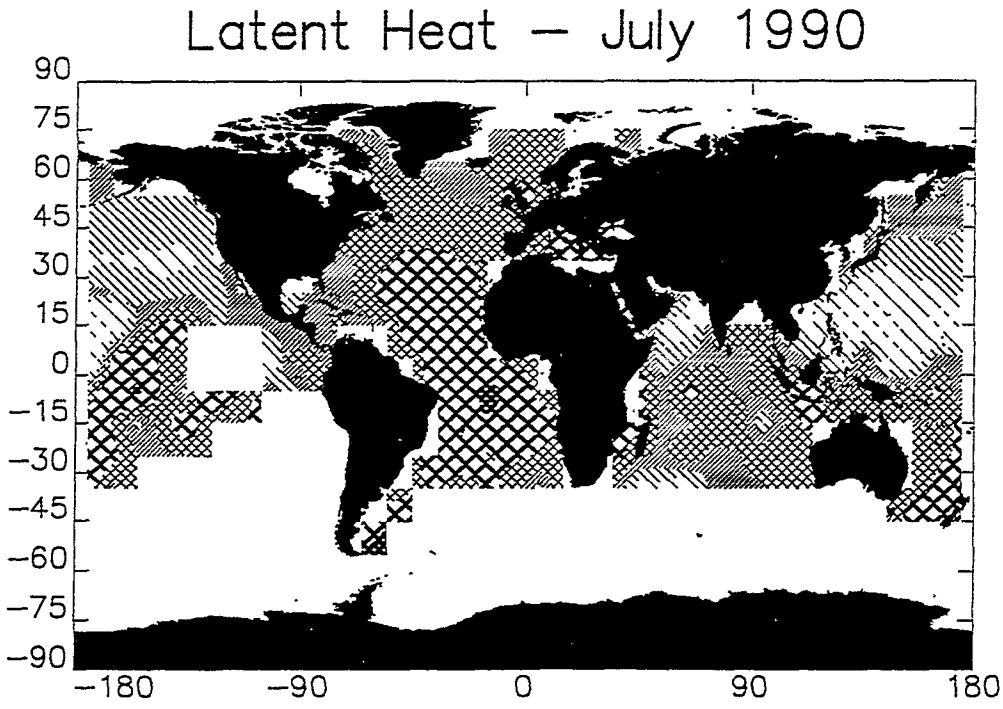

Figure 12 c-d) Global distribution of the difference between the fully corrected and uncorrected latent heat flux fields for January and July 1990. Units Wm^{-2}.

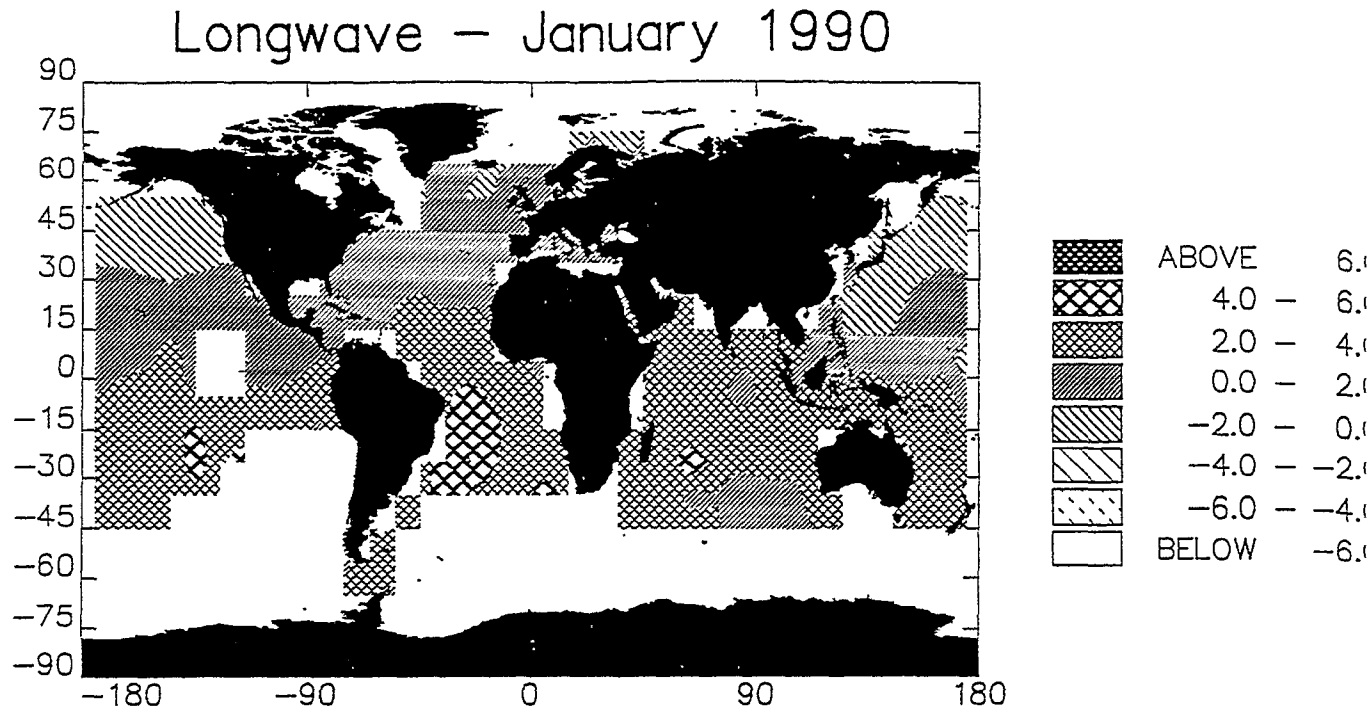

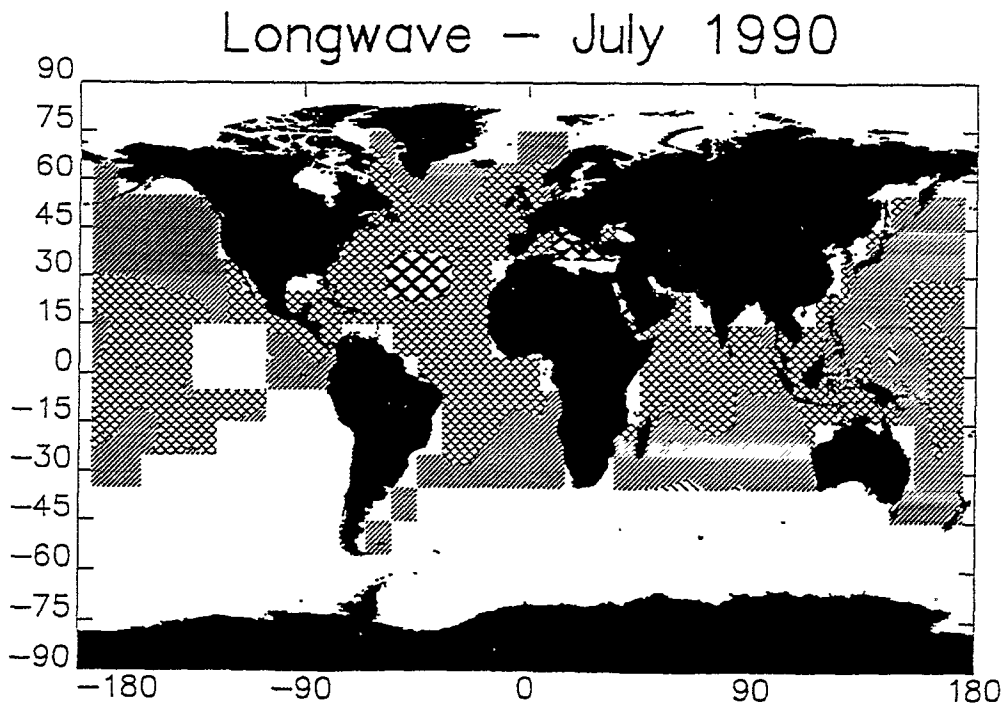

Figure 12e-f) Global distribution of the difference between the fully corrected and uncorrected longwave flux fields for January and July 1990. Units Wm^{-2}.

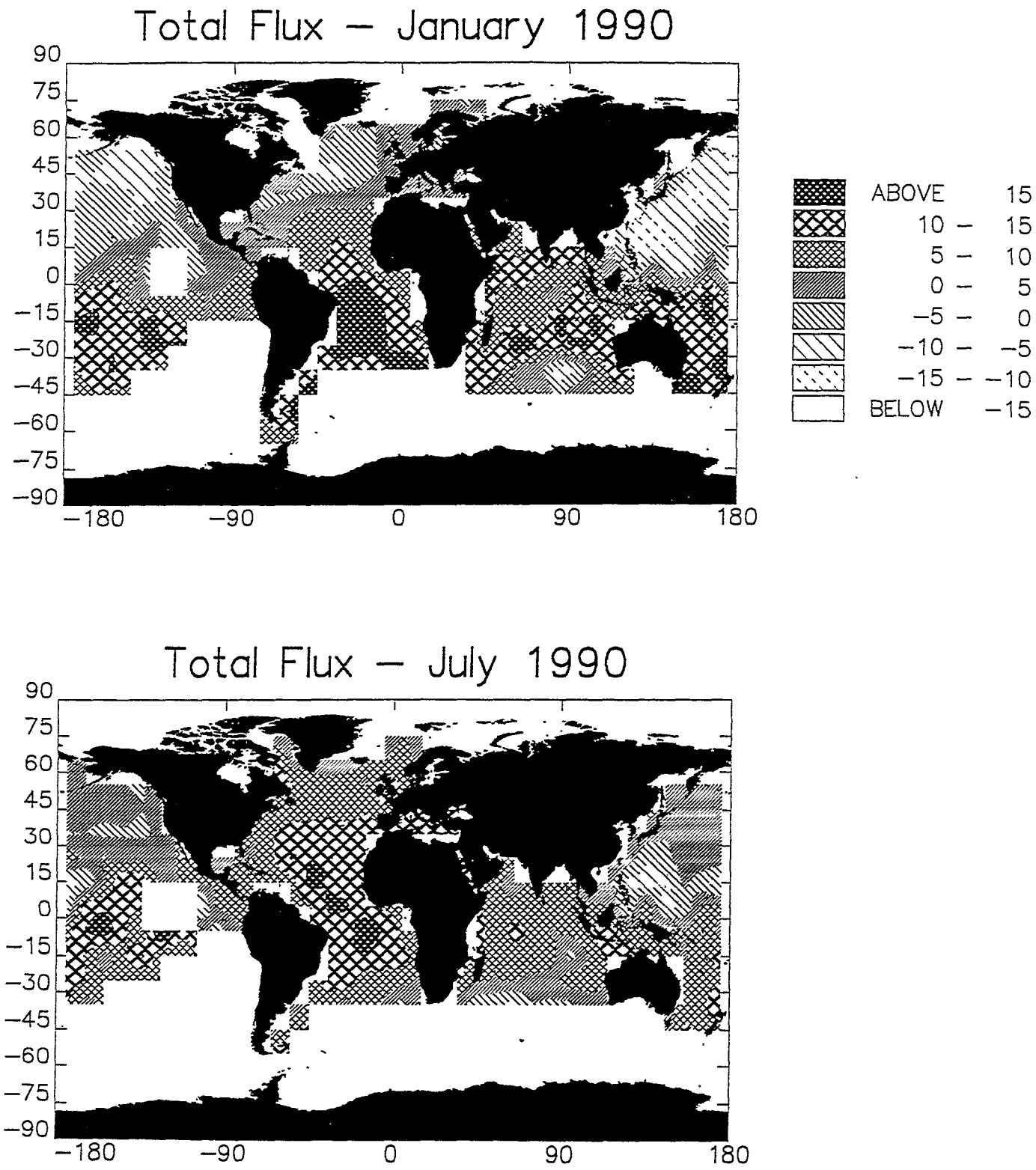

Figure 12g-h) Global distribution of the difference between the fully corrected and uncorrected net heat flux fields for January and July 1990. Units Wm^{-2}.

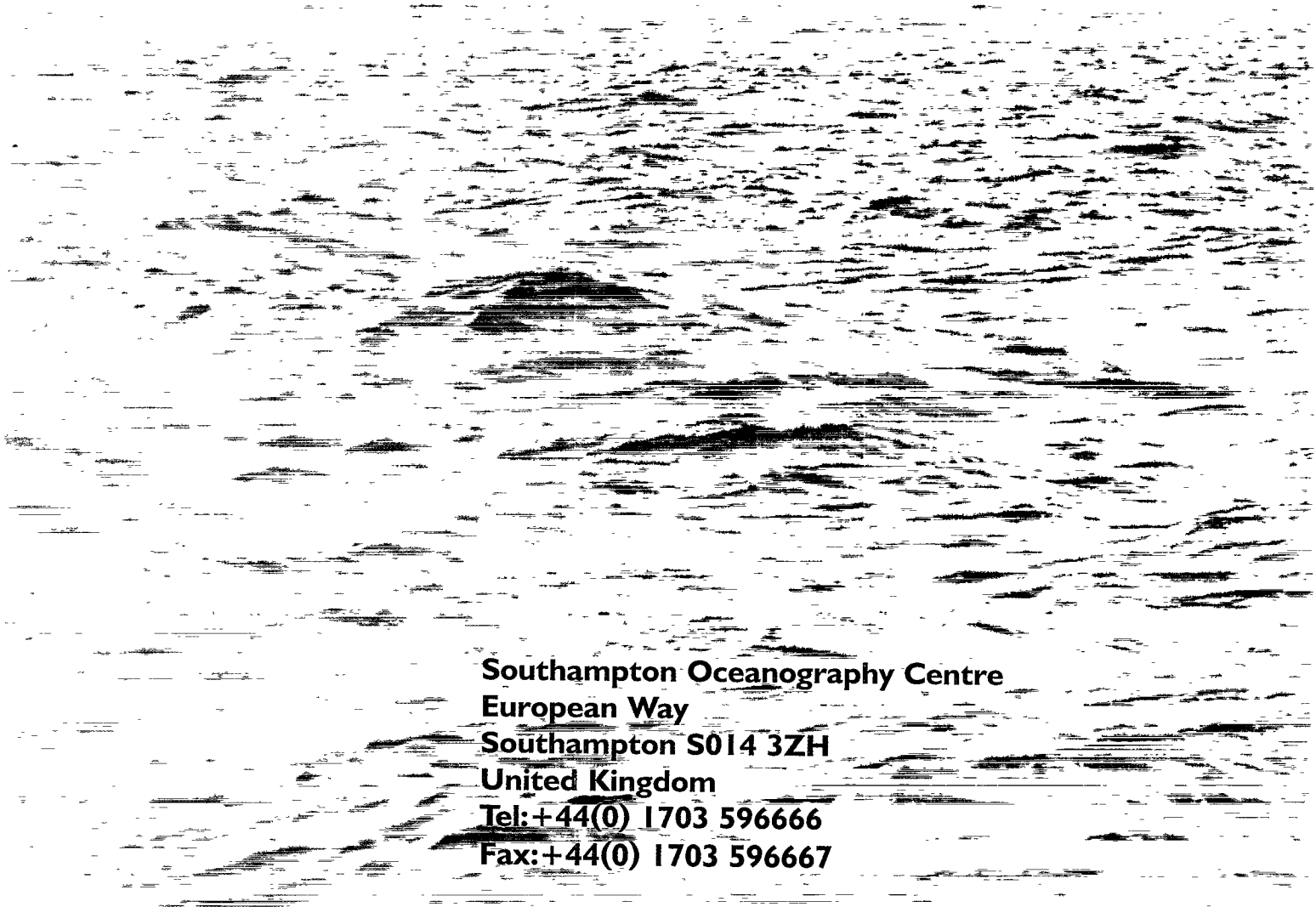

Southampton Oceanography Centre
European Way
Southampton S014 3ZH
United Kingdom
Tel:+44(0) 1703 596666
Fax:+44(0) 1703 596667